PROTEINS: Structure, Function, and Bioinformatics 63:846–867 (2006)

Reconciling the "Old" and "New" Views of Protein Allostery: A Molecular Simulation Study of Chemotaxis Y Protein (CheY)

Mark S. Formaneck, Liang Ma, and Qiang Cui*
Department of Chemistry and Theoretical Chemistry Institute, University of Wisconsin, Madison, Madison, Wisconsin

ABSTRACT **A combination of thirty-two 10-ns-scale molecular dynamics simulations were used to explore the coupling between conformational transition and phosphorylation in the bacteria chemotaxis Y protein (CheY), as a simple but representative example of protein allostery. Results from these simulations support an activation mechanism in which the β4–α4 loop, at least partially, gates the isomerization of Tyr106. The roles of phosphorylation and the conserved Thr87 are deemed indirect in that they stabilize the active configuration of the β4–α4 loop. The indirect role of the activation event (phosphorylation) and/or conserved residues in stabilizing, rather than causing, specific conformational transition is likely a feature in many signaling systems. The current analysis of CheY also helps to make clear that neither the "old" (induced fit) nor the "new" (population shift) views for protein allostery are complete, because they emphasize the kinetic (mechanistic) and thermodynamic aspects of allosteric transitions, respectively. In this regard, an issue that warrants further analysis concerns the interplay of *concerted* collective motion and *sequential* local structural changes in modulating cooperativity between distant sites in biomolecules. Proteins 2006;63:846–867.** © 2006 Wiley-Liss, Inc.

Key words: signal transduction; structural flexibility; allosteric transition; induced fit; population shift; molecular dynamics

INTRODUCTION

Allostery, that is, change in the properties (e.g., conformation) at one site due to an "activation event" (e.g., ligand binding, phosphorylation or adenosine triphosphate [ATP] hydrolysis) at a distant location is central to the function of many biomolecules,[1] especially signaling proteins and large biomolecular assemblies. As a result, the underlying mechanism of allosteric transition has been discussed extensively in terms of both thermodynamic formulations[2–5] and stereochemical models.[6,7] In terms of a stereochemical mechanism, the traditional framework of thinking is based on the "induced fit" model,[8–10] which we refer to as the "old" view here. Being very mechanical in nature, the model envisions that the activation event causes local conformational transitions that are then propagated through the protein via residue–residue interactions to a distant site; the Perutz model for cooperativity in hemoglobin is a classical example,[6] and signaling across > 100 Å in the aspartate receptor of chemotaxis is a more recent case.[9] The underlying implication of the induced fit model is that the propagation occurs through rather well-defined structural pathway(s) and involves specific residues as "signal relays." This is consistent with experimental observations[11–15] that mutations at specific locations can significantly quench or even abolish the allosteric effect. Ranganathan and coworkers have identified "hot spot" residues in a number of classical allosteric systems (hemoglobin, G-protein-coupled receptors, and the PDZ domain family) by statistically analyzing coevolved residues[16–18]; it was proposed that these "hot spot" residues form a network for the propagation of signals in the protein. The existence of a propagation network was demonstrated with NMR relaxation measurements on a small, nonallosteric protein, in which the effect of mutation was observed to propagate as much as 13 Å away through a network of interacting side-chains.[19]

In recent years, the resolution for monitoring conformational transitions in biomolecules has increasingly improved. For example, sophisticated NMR relaxation measurements[20] have made it possible to analyze motions at the microsecond to millisecond time scale with residue resolution during the action of enzymes[21,22] and signaling proteins.[23] Single-molecule fluorescence measurements have identified notable impact on the catalytic function of the hairpin ribozyme due to perturbations 17 Å away.[24] These new experimental developments appear to support a "new" view of allosteric transitions, often referred to as the "population shift" model.[25,26] This model emphasizes that the activated conformation (i.e., the expected confor-

The Supplementary Material referred to in this article can be found online at http://www.interscience.wiley.com/jpages/0887-3585/suppmat/

Grant sponsor: Research Corporation (in support of M. Formaneck); Grant number: RI1039 (to Q. Cui). Grant sponsor: WARF, University of Wisconsin (M. Formenck). Grant sponsor: NIH; Grant number: RO1-GM071428 (Q. Cui).

Q. Cui is an Alfred P. Sloan Research Fellow.

*Correspondence to: Qiang Cui, Department of Chemistry and Theoretical Chemistry Institute, University of Wisconsin, Madison, 1101 University Avenue, Madison, WI 53706.
E-mail: cui@chem.wisc.edu

Received 26 August 2005; Revised 3 November 2005; Accepted 7 November 2005

Published online 10 February 2006 in Wiley InterScience (www.interscience.wiley.com). DOI: 10.1002/prot.20893

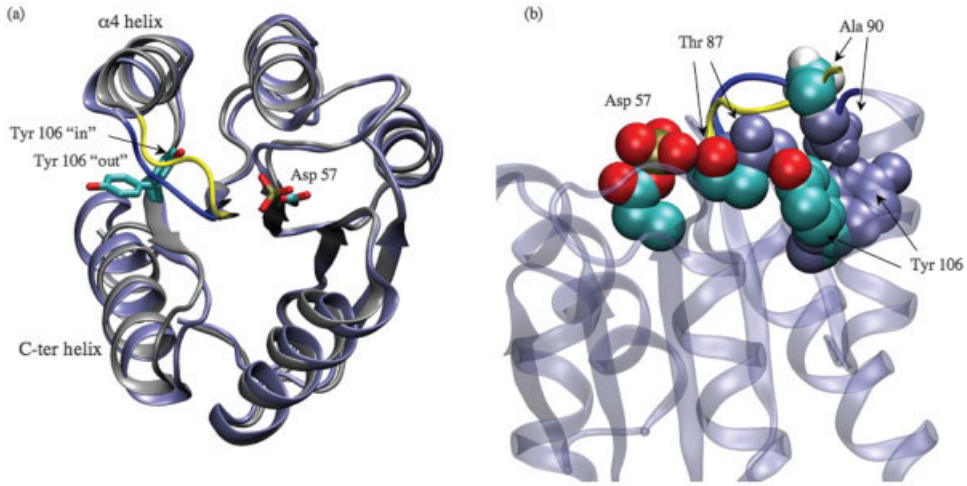

Fig. 1. Comparison of the inactive and active structures of CheY. (**a**) Overlay of the inactive (ice-blue)[37] and active (silver)[38] X-ray structures. The phosphorylation site (Asp57), the response site (Tyr106, "out" position in the inactive structure and "in" position in the active structure) and the key β4−α4 loop (Ala88 to Lys91, dark-blue and yellow for the inactive and active configurations, respectively) are shown. (**b**) Overlay of key residues between the phosphorylation (Asp57) and response sites (Tyr106). Residues in the active structure are colored according to atom types, while those in the inactive structure are ice-blue. The inactive and active configurations of the β4−α4 loop are dark-blue and yellow, respectively. The overall structure of the inactive state is shown in the transparent form as background. The steric interaction between Ala90 and Tyr106 in the inactive structure is clearly visible. The figure was made using VMD.[39]

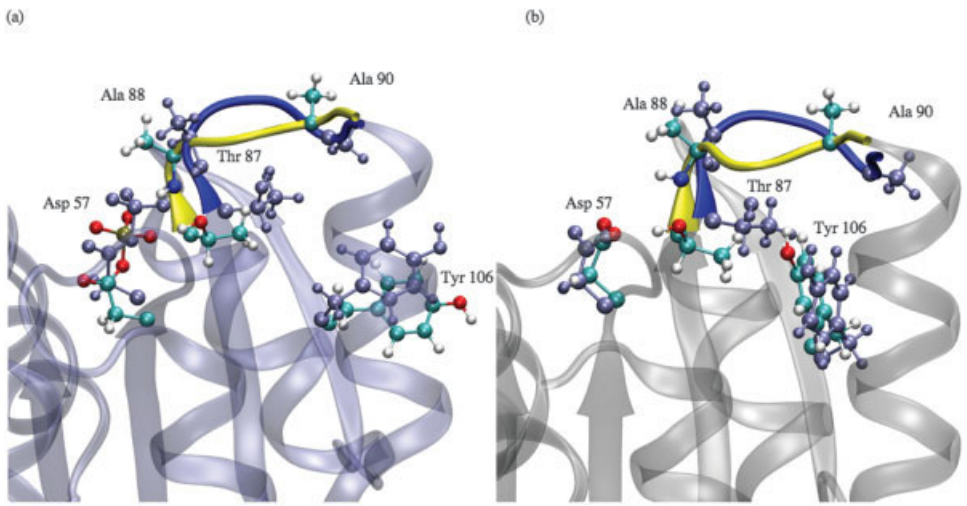

Fig. 5. Spontaneous transition in the β4−α4 loop observed in unbiased simulations, illustrated by overlay of snapshots taken before and after the transition. Color coding is the same as in Figure 1. Residues adopting active-like configurations are color-coded based on atom types, and those adopting inactive-like configurations are ice-blue; the active-(inactive-)like loop configuration is dark-blue (yellow). (**a**) Implicit solvent simulation of the phosphorylated-inactive state; (**b**) explicit solvent simulation of the unphosphorylated-active state.

mation by the end of the allosteric transition) already has a non-negligible population prior to activation, and the activation event merely shifts the pre-existing equilibrium between the inactive and activated conformations, such that the latter becomes the dominant population. The population shift view has gained tremendous popularity over the traditional induced fit paradigm, because the model emphasizes the intrinsic, collective property of the system and does not invoke a *sequential* propagation pathway; indeed, it was argued that in many cases a unique mechanical pathway is not clearly visible between the activation and response sites.[27] A closely related presentation of the population shift model invokes the notion of "redistribution of the conformational ensemble,"[28] which describes the allosteric transition as the consequence of changes in the entire energy landscape, thus redistributing dominant configurations in the conformational ensemble due to the activation event. Algorithms motivated by such a framework have been developed and have been shown to be remarkably successful in describing allosteric phenomena due to various perturbations (e.g., ligand binding,[27,29] pH[30]).

In short, we now have two seemingly contrasting views of allosteric transitions that which apparently differ mainly in two aspects (see Discussion section): (1) the causality between the activation event and emergence of the activated conformation; and (2) whether there exist well-defined structural pathway(s) that couple two distant sites. It is useful to contemplate whether one view is indeed more appropriate than the other, not as an academic exercise, but because establishing the proper framework of thinking is important for identifying factors (e.g., specific residues, interactions and/or overall shape of the biomolecule) that are important to the function of allosteric systems, which has major fundamental as well as practical implications. To this end, it is useful to pick a specific system and analyze the allosteric transition process in detail. Although one should always be cautious about generalizing the results for one system to many, studying a specific system helps to expose points that tend to be overlooked in general discussions.

In this work, we chose to focus on the chemotaxis protein Y (CheY),[31–35] which is a prototypical response regulator in two-component signal trans duction systems.[36] It is highly analogous to the NtrC system studied in the recent NMR experiment[23] that advocated the population shift model; the advantage of studying CheY is the availability of high-resolution NMR and X-ray structures at different states (see below) and the large body of genetic and biochemical data.

As shown in Figure 1, the structure of CheY undergoes rather subtle changes upon the phosphorylation of Asp57; the β4–α4 loop (Ala88 to Lys91) undergoes a major displacement (root-mean-square deviation [RMSD] for backbone and all non-hydrogen atoms is 1.9 Å and 3.6 Å, respectively), and the Tyr106 side-chain switches from being solvent-exposed to being a buried cavity under the β4–α4 loop. It is generally believed that the isomerization of Tyr106 modulates the binding affinity of CheY to Flagella motor switch protein FliM,[38,40] which in turn influences the rotational pattern of the flagella (clockwise [CW] vs. counterclockwise rotation [CCW]) and, consequently, the chemotaxis behavior of bacteria (smooth vs. tumbled swimming).[41] Binding of CheY to FliM favors the CW flagella rotation and tumbled swimming of bacteria. Interestingly, mutation studies on Tyr106 suggest that this residue is not involved in FliM binding yet is important for postbinding activation of the flagellar motor,[42] which confuses the specific role of Tyr106 but still emphasizes its importance in inducing CW rotation of the flagella. The distance between Tyr106 and the phosphorylation site (Asp57) is more than 9.5 Å (based on Cα atoms), which makes CheY a prototypical single-domain protein that exhibits allosteric behavior.[23,43,44]

The highly conserved Thr87 spatially separates Asp57 and Tyr106.[45] Therefore, the traditional activation mechanism of CheY is the so-called "Y–T" coupling scheme[38,46,47]: Phosphorylation of Asp57 causes Thr87 to move toward the phosphorylation site due to enhanced hydrogen-bonding in teraction, which leaves more space for Tyr106 to occupy the buried rotameric state. This widely-accepted "Y–T" coupling scheme, which is reminiscent of the induced fit view of allosteric transition, is consistent with the fact that Thr87 is a conserved residue in not only CheY but also many other response regulators (e.g., FixJ[48] and Spo0A[49]).

However, there is also evidence in favor of the "new" view. Similar to nitrogen regulation protein, NtrC,[23] partial activation of CheY was observed even in the absence of phosphorylation; specifically, 14% CW rotation of isolated flagella with unphosphorylated CheY was observed, compared with 100% CCW rotation in the absence of CheY.[50] In addition, although Thr87 is a conserved residue, mutations that replaced it with even Ala kept partial activity.[51] Finally, multiple orientations of Tyr106 were found in several X-ray studies of CheY in the absence of phosphorylation.[37,52] This was shown more clearly in the high-resolution X-ray structure[37] at 1.1 Å resolution. In this "meta-active" structure, the side-chain of Tyr106 was found to occupy both the solvent-exposed and the buried positions, while only one side-chain position consistent with the earlier study[52] was found for Thr87, suggesting that the steric interaction between Thr87 and the buried rotamer of Tyr106 is actually minimal. These observations support a population shift view of CheY activation,[37] in which phosphorylation merely shifts the pre-existing equilibrium between the solvent-exposed and buried populations of Tyr106 toward the latter. Based on subtle changes in the β4–α4 loop observed in the "meta-active" structure, it was speculated that this loop might be involved in regulating the Tyr106 transition, and that the role of Thr87 and phosphorylation is to modulate the loop configuration.[37] This interesting hypothesis was partially supported by a simulation study of the related response regulator, FixJ, which showed that pushing the loop toward the active configuration induced the transition of the Tyr106 equivalent (Phe101).[53] The simulation protocol used in that study, however, was rather crude (in vacuum). Moreover, the correlation between the loop configuration and phosphorylation/Thr87 was not explicitly shown.

In short, it is striking that even in relatively simple allosteric systems such as CheY, both the induced fit and population shift views can be proposed. The small size and modest degree of conformational rearrangements of CheY make it an ideal system for molecular dynamics simulation study at the atomic level. In particular, we used various types of molecular dynamics simulations to better understand the role of the β4–α4 loop and to explore other possibly important factors in CheY activation; the results were discussed in the context of comparing and consolidating the "old" and "new" views for allosteric transitions in general.

RESULTS

In this section, we first report the behavior of CheY starting from different chemical and conformational states (Table I) in unbiased simulations that reflect the intrinsic properties of the system and its response to perturbations (phosphorylation or mutation) at the nanosecond time scale. We then present results from biased molecular

TABLE I. Characteristics for the Starting Configuration in Unbiased Molecular Dynamics Simulations

Set	Asp 57 Chemical State[a]	Conformation[b]	Residue 87	Tyr106[c]	PDB code[d]
1	UnP	Inactive	Thr	Out	1JBE
2	P	Inactive	Thr	Out	1JBE
3	UnP	Active	Thr	In	1F4V
4	P	Active	Thr	In	1F4V
5	UnP	Meta-active	Thr	In	1JBE
6	P	Inactive	Ala	Out	1JBE
7	P	Active	Ala	In	1F4V

[a]UnP and P refer to unphosphorylated and phosphorylated Asp57, respectively.
[b]The conformational state is mainly characterized by the orientation of the β4–α4 loop and position of the Tyr106 side chain (see Fig. 1).
[c]Out and In refer to the solvent-exposed and buried rotameric state of the Tyr106 side chain, respectively (see Fig. 1).
[d]1JBE is based on Simonovic and Volz[37] and 1F4V is based on Lee et al.[38] In the T87A mutant simulations (Sets 6 and 7), the side chain of Thr87 was modified to a methyl group based on the corresponding wild-type X-ray structures.

dynamics (BMD) simulations, in which a specific component of the system is subject to a conformational bias; the results report on the coupling between different structural motifs and provide hints on factors that might be important to the allosteric transition. Although multiple simulations were performed with each setup, only representative results are shown in the main text; the complete collection of simulation results are included in the Supplemental Material.

Unbiased Molecular Dynamics Simulations

Since the conformational transitions in CheY are relatively localized, the properties of interest focus on the region close to the phosphorylation site (Asp 57) and the transition site (Tyr106); these include χ_1 of Tyr106, hydrogen-bonding interactions involving the carboxylate or the phosphate group of Asp57, and the conformation of the β4–α4 loop. We characterize the conformation of the β4–α4 loop with the ΔRMSD coordinate as defined in Eq. (1) in the Computational Methods section, where the RMSDs involve all backbone atoms in residues Ala88–Lys91; positive (negative) ΔRMSD values imply that the loop is closer to the inactive (active) X-ray configuration. Another variable found useful is the pseudodihedral angle involving the Cα atoms in Thr87–Ala90, which was also used in a previous MD study of the related system FixJ[53]; the inactive and active loop configurations in the CheY X-ray structures have values of ~14° and ~113°, respectively.

Wild-type simulations

When the initial structure of the MD simulation involved a chemical state of Asp57 that was consistent with the original X-ray structure [i.e., the unphosphorylated-inactive conformation (Set 1 in Table I) and the phosphorylated-active conformation (Set 3)], the system remained similar to the initial structure throughout the 10-ns scale simulations, with rather moderate variations depending on the solvent model and initial velocity distribution.

In the explicit solvent simulations, when Asp57 was unphosphorylated in the inactive state (Set 1), χ_1 of Tyr106 [Fig. 2(a)] remained close to the initial value of 60°, with occasional transition to −60° that corresponds to a different solvent-exposed rotameric state of Tyr106. The carboxylate of Asp57 remained far from the OH group of Thr87 and backbone NH of Ala88 [Fig. 2(b)], which are the two residues that interact with phoshphorylated Asp57, as observed in the active X-ray structure.[38] The β4–α4 loop remained closer to the X-ray inactive configuration, as the ΔRMSD remained close to +1.0 Å [Fig. 2(c)] and the loop pseudodihedral stayed around 0° [Fig. 2(d)] in the majority of the simulations. The implicit solvent simulations exhibited very similar behaviors (Figs. S2–S4 in Supplementary Materials), although the χ_1 transition between 60° and −60° in Tyr106 was more frequent; the β4–α4 loop more often sampled configurations with ΔRMSD close to zero or even slightly negative, although the inactive configuration was clearly much more populated, as also indicated by the values of the loop pseudodihedral angle.

In the phosphorylated-active (Set 3) simulations, it was the implicit solvent results that displayed a "tighter" structure for which the χ_1 of Tyr106, hydrogen bonding between the phosphate and Thr87/Ala88, as well as the ΔRMSD and pseudodihedral angle of the β4–α4 loop all remained similar to the initial structure throughout multiple ~10-ns simulations (Figs. S6–S8 in Supplementary Materials). With the explicit solvent simulations, however, the system exhibited larger fluctuations in the phosphate hydrogen-bonding pattern and configuration of the β4–α4 loop. As shown in Figure 3(b), the hydrogen bond between the phosphate and NH of Ala88 constantly formed and broke during the simulation, because both groups can be equally stabilized by the explicit solvent molecules. At the same time, the β4–α4 loop exhibited larger fluctuations in both ΔRMSD [compare Figs. 2(c) and 3(c)] and the pseudodihedral angle [compare Figs. 2(d) and 3(d)]; for example, ΔRMSD often reached +1.0 Å although the active configuration was more populated.

When the chemical state of Asp57 was changed from that in the original X-ray structure [i.e., in the phosphorylated-inactive (Set 2) and unphosphorylated-active (Set 4) simulations], the behavior of the system seemed to be more sensitive to the solvent model. The difference, however, was reproducible and straightforward to rationalize (see Discussion section).

In the phosphorylated-inactive (Set 2) simulations, the system remained inactive-like throughout the 7-ns explicit solvent MD (Figs. S9–S10 in Supplementary Materials); all key properties, including the hydrogen-bonding pattern of Asp57 and the β4–α4 loop configuration, were in fact very similar to the unphosphorylated-inactive simulations (Fig. 2). With the Generalized Born with switching function (GBSW) implicit solvent model, by contrast, the β4–α4 loop underwent substantial displacements, such that both Thr87 and Ala88 formed stable hydrogen bonds

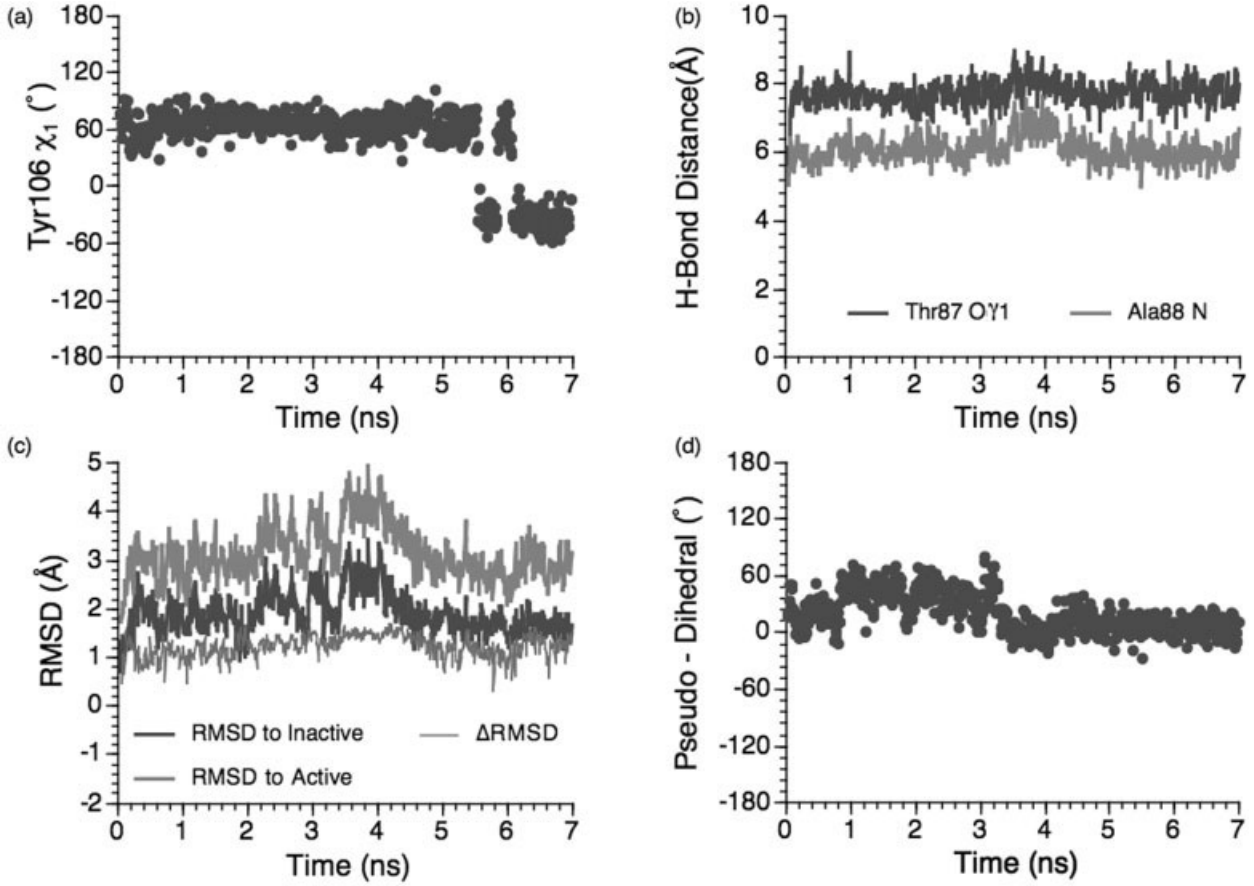

Fig. 2. Key properties during one unbiased explicit solvent simulation of the unphosphorylated-inactive state (Set 1 in Table I). (**a**) χ_1 of Tyr106; (**b**) two key hydrogen-bonding distances, measured as the shortest distances between the oxygen atoms in Asp57, and the Oγ in Thr87 and backbone N in Ala88, respectively; (**c**) the RMSD in the backbone of the β4–α4 loop (Ala88–Lys91) relative to the inactive[37] and active[38] X-ray configurations, as well as the differential RMSD. A positive (negative) ΔRMSD indicates that the loop is closer to the inactive (active) configuration; (**d**) the pseudodihedral angle based on the Cαatoms in Thr87–Ala90.

with the phosphate group [Fig. 4(b)]. The degree of loop transition varied in three independent GBSW simulations, but all had ΔRMSD remain negative for a majority of the 9-ns simulations [Fig. 4(c)]; the pseudodihedral also increased from ~0° to ~120° [Fig. 4(d)]. The most striking transition observed is shown structurally in Figure 5(a), where the changes in key motifs, especially the β4–α4 loop, are evident. Nevertheless, Tyr106 remained in the solvent-exposed rotameric state throughout these simulations [Fig. 4(a)].

In the unphosphorylated-active (Set 4) simulations, the opposite trend was observed. The structure remained active in the GBSW simulations (Figs. S15–S18 in Supplementary Materials), although the hydrogen bond between Ala88 NH and Asp57 was broken in one simulation (Fig. S15 in Supplementary Material), which was correlated with the ΔRMSDs' occasional sampling of positive values; the loop pseudodihedral angle remained close to the active value of ~100°. In the explicit solvent simulations; by contrast, both hydrogen bond donor groups (OH in Thr87 and NH in Ala88) broke interactions with Asp57 during multiple simulations [Fig. 6(b)], and the β4–α4 loop became very similar to the inactive configuration [ΔRMSD ~ +1 Å in Fig. 6(c); the pseudodihedral approached ~0° in Fig. 6(d)]; an example for the transition is illustrated structurally in Figure 5(b). Tyr106, however, remained in the buried rotameric state throughout these simulations [Fig. 6(a)].

Finally, the "meta-active" simulation (with explicit solvent, Set 5), in which Tyr106 was found experimentally to adopt the buried state without phosphorylation, showed that the β4–α4 loop remained in the inactive configuration [according to the ΔRMSD and pseudodihedral angle shown in Fig. 7(c and d)], as observed in the X-ray structure,[37] and both Thr87 and Ala88 remained distant from Asp57 throughout the simulations [Fig. 7(b)]. The same trend was found in implicit solvent simulations (see Figs. S19–S20 in the Supplementary Materials). Apparently, Tyr106 did not suffer from any major steric repulsion from Thr87, as speculated in the "Y–T" hypothesis.[46]

T87A mutant simulations

When Thr87 was replaced by Ala, the β4–α4 loop transition toward the active configuration was not observed when the inactive structure was phosphorylated, even with the implicit solvent model [Fig. 8(c and d)]. The

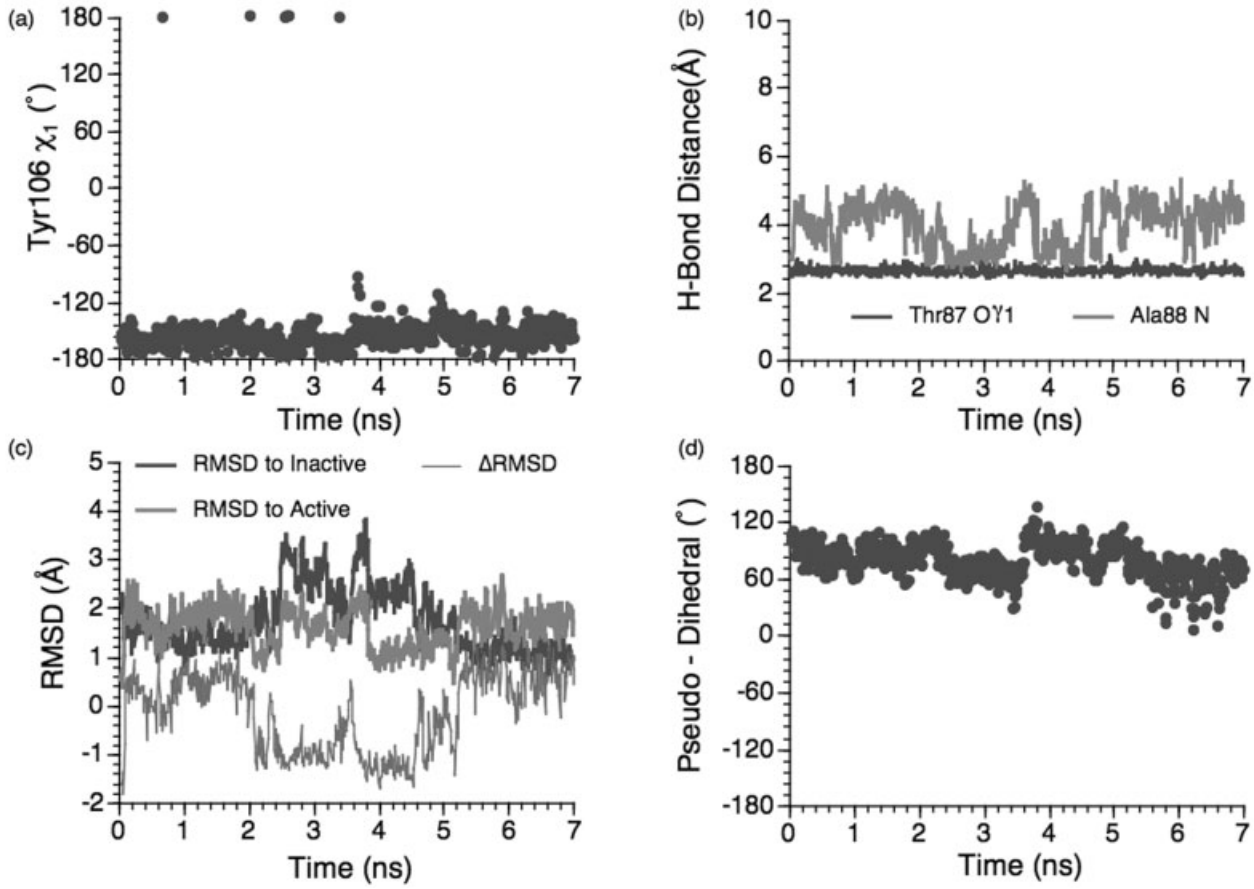

Fig. 3. Key properties during one unbiased explicit solvent simulation of the phosphorylated-active state (Set 3 in Table I). See Figure 2 caption for notations. Note the large fluctuations in the β4–α4 loop and hydrogen-bonding distance between Ala88 N and phosphate compared to the unphosphorylated-inactive simulations (Fig. 2) and implicit solvent simulations (Figs. S6–S8 in Supplementary Material).

hydrogen bond between the NH of Ala88 and phosphate formed in the beginning of the simulation but broke after about 5 ns [Fig. 8(b)]. Apparently, without the collaborative effort from the OH in Thr87, the backbone of Ala88 was not able to form a stable hydrogen bond with the phosphate, which is required to stabilize the loop transition.

In the phosphorylated-active simulations of the T87A mutant with explicit solvent, the hydrogen bond between Asp57 and Ala88 NH broke in the early stage of the simulation [Fig. 9(b)], which resulted in the transition of the β4–α4 loop toward the inactive configuration, as indicated by the positive values of ΔRMSD [Fig. 9(c)]; the loop pseudodihedral angle oscillated wildly in a wide range [Fig. 9(d)]. The different behavior from the wild-type phosphorylated state once again highlights the importance of forming both hydrogen-bonding interactions (Thr87, Ala88) to stabilize the β4–α4 loop in the active configuration.

Biased Molecular Dynamics (BMD) Simulations

Biasing the β4–α4 loop

In seven BMD simulations, the "out → in" transition of Tyr106 was observed in two trajectories within ~4 ns, highlighting the complexity of the process. In the two successful simulations, the sequence of events are similar; important structural parameters and snapshots from one trajectory are shown in Figures 10 and 11, respectively. Since all BMD simulations were carried out using the GBSW implicit solvent model and started with random snapshots from the unbiased phosphorylated-inactive (Set 2) simulations, the hydrogen bonding between Thr87, Ala88, and the phosphate was intact throughout the BMD simulation (see above subsection), although the hydrogen bonding involving Ala88 was somewhat less stable [Fig. 10(b)]. In addition to Ala90 in the β4–α4 loop, two residues (Ile95 and Val108) were found to form a "doorway" for the entry of Tyr106 into the buried conformation. As shown in Figure 1(a), Ala90 in the inactive loop configuration blocks the rotation of Tyr106 sterically. Ala90 also interacts with the two doorway residues. As the β4–α4 loop was pushed toward the active configuration, Ala90 moved out of the way, and the two doorway residues were able to come closer to each other, forming hydrophobic interactions [Fig. 11(b)]. As a result, Tyr106 could not isomerize readily, and χ_1 remained close to 60° even after the displacement of Ala90 [Figs. 10(a) and 11(b)]. As the loop moved further, the doorway residues opened up [Fig.

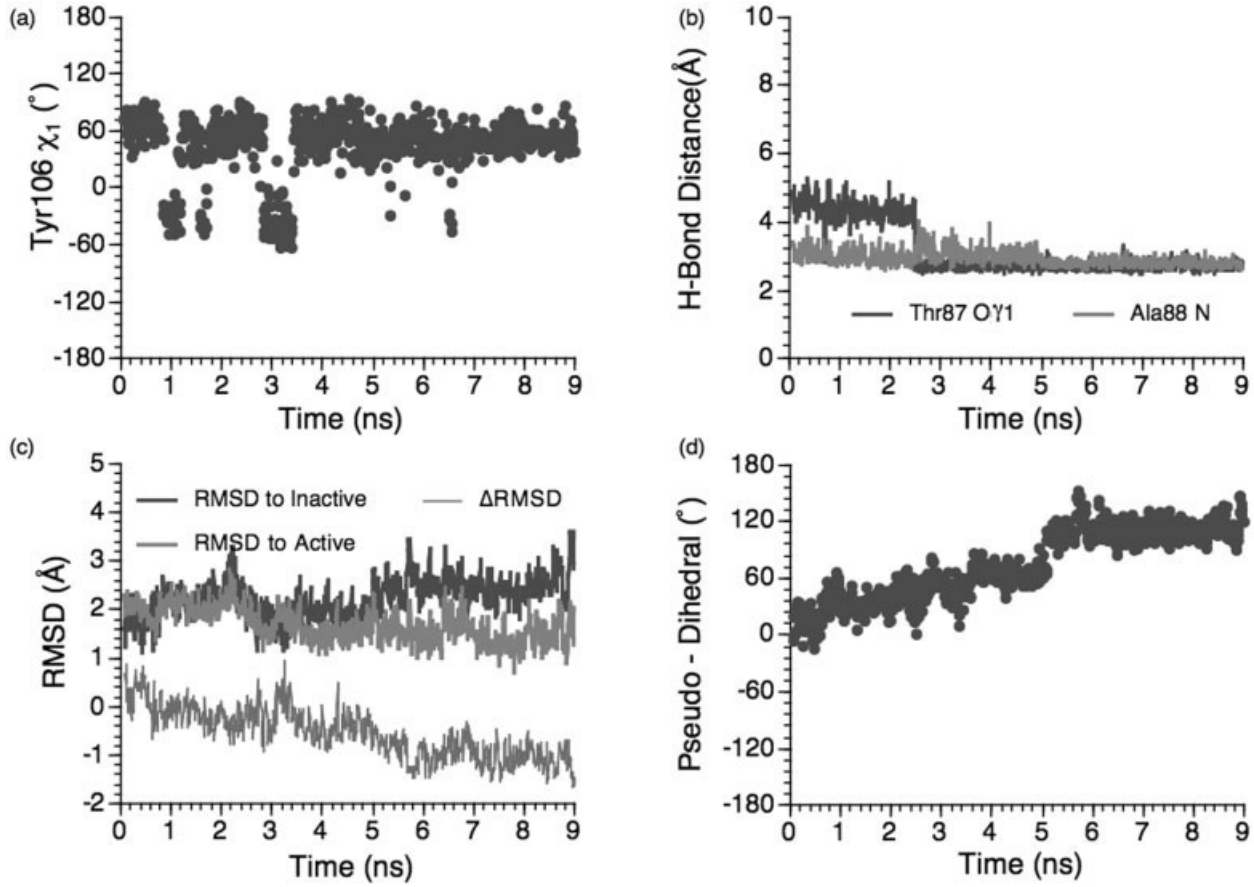

Fig. 4. Key properties during one unbiased implicit solvent simulation of the phosphorylated-inactive state (Set 2 in Table I). See Figure 2 caption for notations. Note the spontaneous transition of the β4–α4 loop toward the active configuration, as indicated by ΔRMSD and the pseudodihedral angle.

11(c)], although the magnitude of doorway size (as measured by the minimal distance between Val108 and Ile95 non-hydrogen atoms) only increased slightly [Fig. 10(d)]. This eventually allowed the entry of the Tyr106 side chain [Figs. 10(a) and 11(d)]. Since Tyr106 fitted nicely into the cavity formed by the doorway residues and the β4–α4 loop, the out → in transition, once allowed sterically, occurred rather quickly, within 1 ns; the doorway width increased at ~1.6 ns [Fig. 10(d)] and the Tyr106 transition occurred at ~2.6 ns [Fig. 10(a)]. It is worth noting that Tyr106 made a transition to a position half way to the buried site, as indicated by its intermediate value of solvent-accessible surface area.

Biasing Tyr106

With Tyr106 explicitly driven from the solvent-exposed to the buried orientation, the motif that displayed the most significant perturbation was, as somewhat expected, the β4–α4 loop. As shown in Figure 12, as Tyr106 makes the transition toward the buried position [~1.1 ns; Fig. 12(a)], the ΔRMSD exhibited a visible dip [Fig. 12(c)] and the loop pseudodihedral angle increased significantly [Fig. 12(d)], indicating that part of the loop was moving toward the active configuration. This is largely induced by the steric clash between Tyr106 and Ala90, which caused a brief positioning of Ala90 and Glu89 in the active position, and a slight distortion of the internal structure of the loop; the situation is shown structurally in Figure 13. After this rearrangement, however, the loop did not move further toward the active configuration, and ΔRMSD returned to being mostly positive, and the pseudodihedral angle remained around 0°. This is not unexpected, because Asp57 was not phosphorylated in the simulation, and both Thr87 and Ala88 remained far from Asp57 [Fig. 12(b)]. Therefore, once Tyr106 adopted the buried orientation, the loop was not driven or stabilized to adopt the active conformation. In fact, these observations are consistent with the "meta-active" X-ray structure,[37] in which Tyr106 adopts the buried position, while both the β4–α4 loop and Thr87 have essentially the inactive configurations.

Binding Free Energy of Tyr106

Not surprisingly, the binding free energy of the solvent-exposed Tyr106 side chain to CheY was found to depend very little on the protein conformation (Table II). The interesting and somewhat unexpected result is that the same trend was found for the buried Tyr106: Very similar binding free energy was estimated for the "meta-active" and "active" states; compared to the solvent-exposed conformation, the buried rotamer has smaller electrostatic inter-

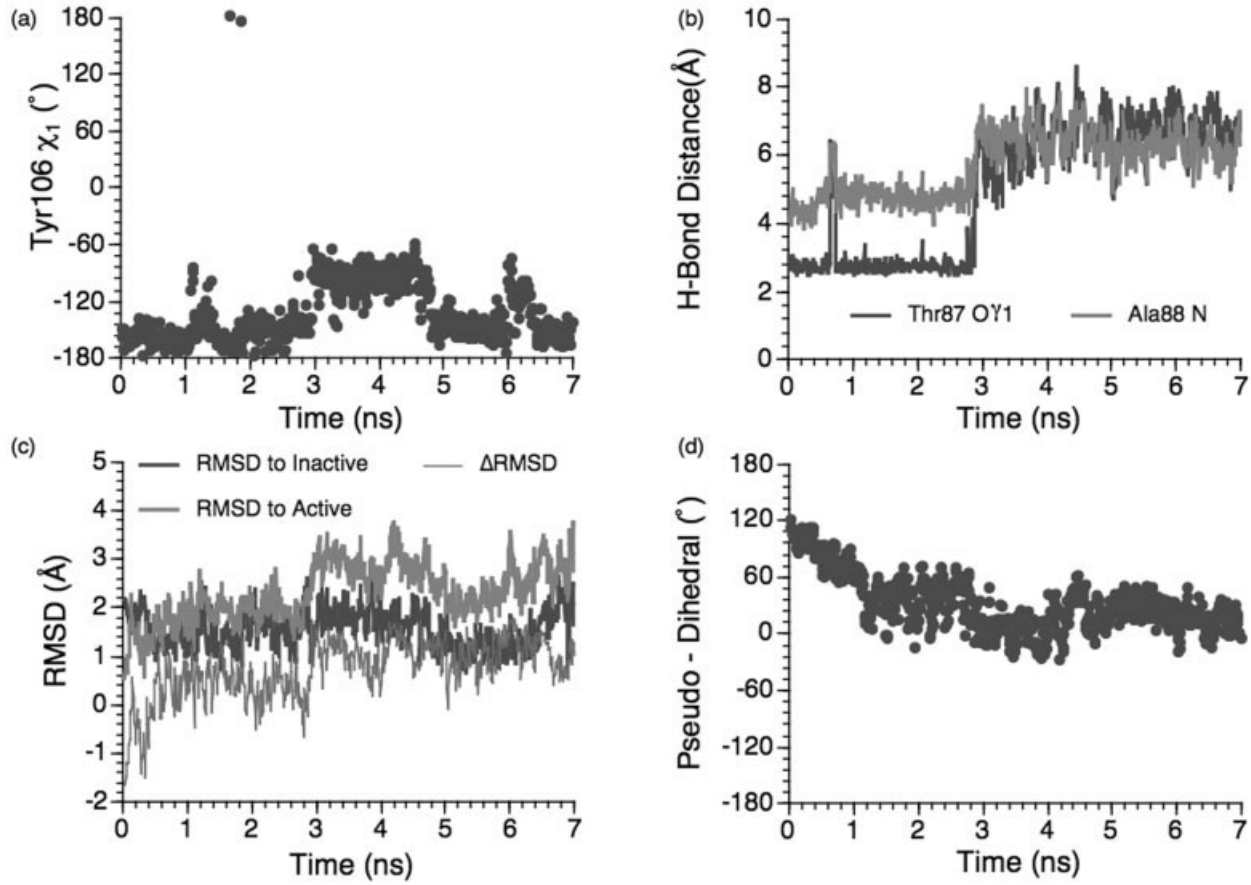

Fig. 6. Key properties during one unbiased explicit solvent simulation of the unphosphorylated-active state (Set 4 in Table I). See Figure 2 caption for notations. Note the spontaneous transition of the β4–α4 loop toward the inactive configuration, as indicated by ΔRMSD and the pseudodihedral angle.

actions but more favorable van der Waals (vdW) interactions with the environment, which is consistent with the hydrophobic character of the binding site (Fig. 1). The small dependence of binding on the loop configuration suggests that the β4–α4 loop does not make any major contribution to the stability of Tyr106 once it is buried. In addition, this semiquantitatively confirms the conclusion from the "meta-active" MD simulations that there is minimal steric interaction between the buried Tyr106 and Thr87, even when the latter adopts the inactive position.

Normal Mode Analysis

The low-frequency modes of the inactive-unphosphorylated CheY indicate that the most mobile regions include the β4–α4 loop, and the α4, and the C-terminal helices. For example, all these regions showed motion in the lowest frequency mode [Fig. 14(a)]. The second mode [Fig. 14(b)] involves essentially only the bending of the C-terminal helix at residue 118. In mode 3 [Fig. 14(c)] and mode 4 [Fig. 14(d)], both the β4–α4 loop and the α4 helix exhibited significant motion, while the rest of the structure remains essentially intact.

Unlike several multidomain systems analyzed in previous studies,[55–57] the involvement coefficients in the single-domain CheY do not exhibit highly distinct features and distribute rather evenly among low-frequency modes; somewhat similar behavior was found in a previous study of a small signaling protein, *ras* p21.[58] For the overall involvement coefficients [Fig. 15(a)], mode 2, which largely involves the bending of the C-terminal helix [Fig. 15(b)], has a large contribution of 0.3; many other modes have fairly comparable contributions. Indeed, the cumulative overall involvement coefficient [Fig. 15(c)] is only ~0.3 with 50 lowest-frequency modes. The situation is similar for the local involvement coefficients for the β4–α4 loop transition [Fig. 15(b and d)]. Clearly, the inactive → active β4–α4 loop transition is rather complex structurally and not naturally coded in the three-dimensional (3D) structure of CheY; this is not entirely unexpected for a rather localized transition, in contrast to domain motions in larger systems.[55–57]

DISCUSSION

Allosteric transitions are difficult to study both experimentally and computationally due to the involvement of a large number of degrees of freedom and motions occurring at different spatial and time scales. In this work, we chose to use a single-domain signal transduction protein, CheY, as a model system to contemplate different views of allosteric transition mechanisms.[8–10,25,26] Even for such a

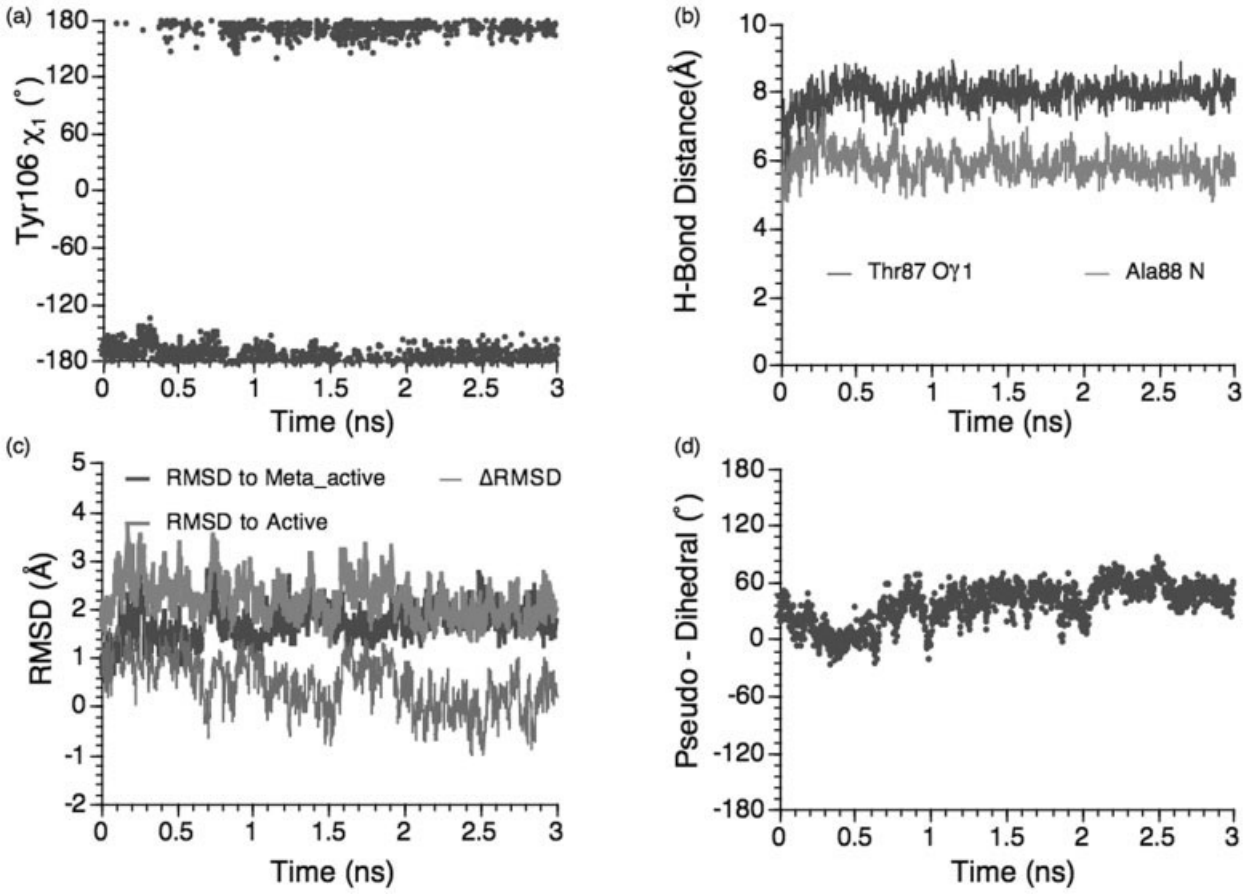

Fig. 7. Key properties during one unbiased explicit solvent simulation of the unphosphorylated-meta-active state (Set 5 in Table I). See Figure 2 caption for notations.

small system with a relatively modest degree of conformational rearrangements, the process was found to be rather complex and difficult to characterize quantitatively. Instead, we used a combination of molecular simulations under different conditions as "computational probes" to deduce the structural motifs and interactions that are potentially important to the activation of this prototypical response regulator protein.

Y–T COUPLING

Although the traditional "Y–T" coupling scheme[46] is very logical and consistent with the fact that Thr87 is a conserved residue in CheY[45] and in many response regulators,[59] it is contradictory to the observation of the "meta-active" X-ray structure,[37] in which Tyr106 occupies the buried position, without Asp57 being phosphorylated and Thr87 being displaced. The current unbiased MD simulations further confirmed that the "meta-active" structure is unlikely an artifact due to crystalization condition, and the observed electron density at the buried site does not need to be interpreted as solvent.[52] Moreover, the steric interaction between the buried Tyr106 and Thr87 in the inactive position is minimal, which is reflected by the fact that Thr87 did not move significantly in either the unbiased "meta-active" MD simulations or biased simulations in which Tyr106 was pushed into the buried position; semi-quantitatively, the binding free energy of Tyr106 in the "meta-active" state was found to be similar to that in the phosphorylated active structure (Table II).

Activation Through a Gating β4–α4 Loop

Evidently, an alternative mechanism is needed to describe the activation of CheY (and related response regulators), and to explain the conservation of Thr87 in those proteins. Motivated by the fact that the β4–α4 loop undergoes a significant displacement from the inactive to the active X-ray structures and that Ala 90 in the inactive-loop configuration blocks the rotation of Tyr106 (Fig. 1), an alternative activation mechanism was hypothesized,[37] in which the rotation of Tyr106 is, at least partially, gated by the conformation of the β4–α4 loop, and the role of the conserved Thr87 is to shift the population of this loop toward the active configuration when Asp57 is phosphorylated. It was this hypothesis that drove the design of all the molecular simulations reported above. In the following, we scrutinize the major findings in the simulations and show that the hypothesis is indeed consistent with all the simulation results and available experimental data on CheY.

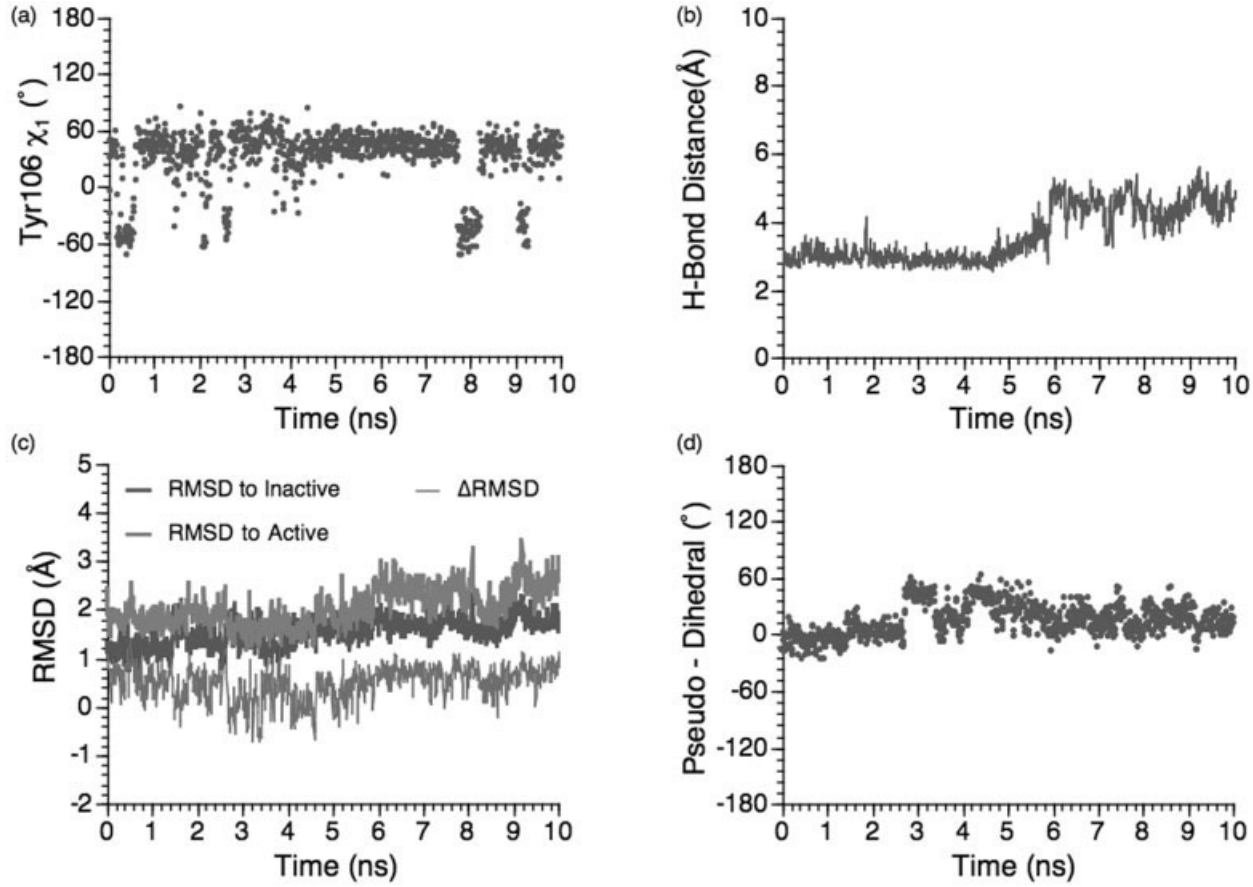

Fig. 8. Key properties during one unbiased implicit solvent simulation of the unphosphorylated-inactive state of the T87A mutant (Set 6 in Table I). See Figure 2 caption for notations. Note that the spontaneous loop transition found in the wild-type (Fig. 4) was no longer observed.

Coupling between the β4–α4 loop and Thr87 displacement

It is worth noting that although implicit and explicit solvent simulations sometimes produced different behaviors in the β4–α4 loop and Thr87, the results actually consistently support the role of Thr87 in stabilizing the active configuration of this loop. For example, the β4–α4 loop was found to make a transition toward the active configuration in the phosphorylated-inactive simulations only with the *implicit* solvent model, while the reverse loop transition was observed in the unphosphorylated-active simulations only with the *explicit* solvent model. This apparent difference cannot be explained by the neglect of solvent collision in the implicit solvent simulation (thus, natural "speed up" for conformational transitions[60]), since it was in the explicit solvent simulation that a transition was observed for the unphosphorylated-active state. Rather, the results suggest that electrostatic interactions involving solvent-exposed groups (e.g., Asp57) were overestimated by the implicit solvent model used here, since hydrogen bonding to solvent molecules was no longer possible; this has also been noted repeatedly in previous studies.[61–63] Specifically, the hydrogen bonding between Thr87 and Asp57 was overestimated by the GBSW model, which in turn overstabilized the active configuration of the β4–α4 loop. This explained why the loop transition was observed in the phosphorylated-inactive simulations but not in the unphosphorylated-active simulations when GBSW was used. Due to a similar reason, the loop was found to remain much closer to the active configuration in the GBSW simulations of the phosphorylated-active state, while larger fluctuations were observed in the explicit solvent simulations; this is because a key hydrogen-bonding interaction between the phosphate and the NH of Ala88 could be replaced by interactions between these groups and explicit solvent molecules.

The role of Thr87 in stabilizing the β4–α4 loop is also supported by the T87A mutant simulations. The loop transition toward the active configuration was *not* observed in multiple phosphorylated-inactive simulations even with the GBSW model, and the loop became very close to the *inactive* configuration in the phosphorylated-active simulation with the explicit solvent model. Clearly, the mutation has abolished an important factor that stabilizes the active configuration of the β4–α4 loop, and the NH of Ala88 itself is not sufficient to make the active configuration the dominant loop population even in the presence of the phosphate on Asp57.

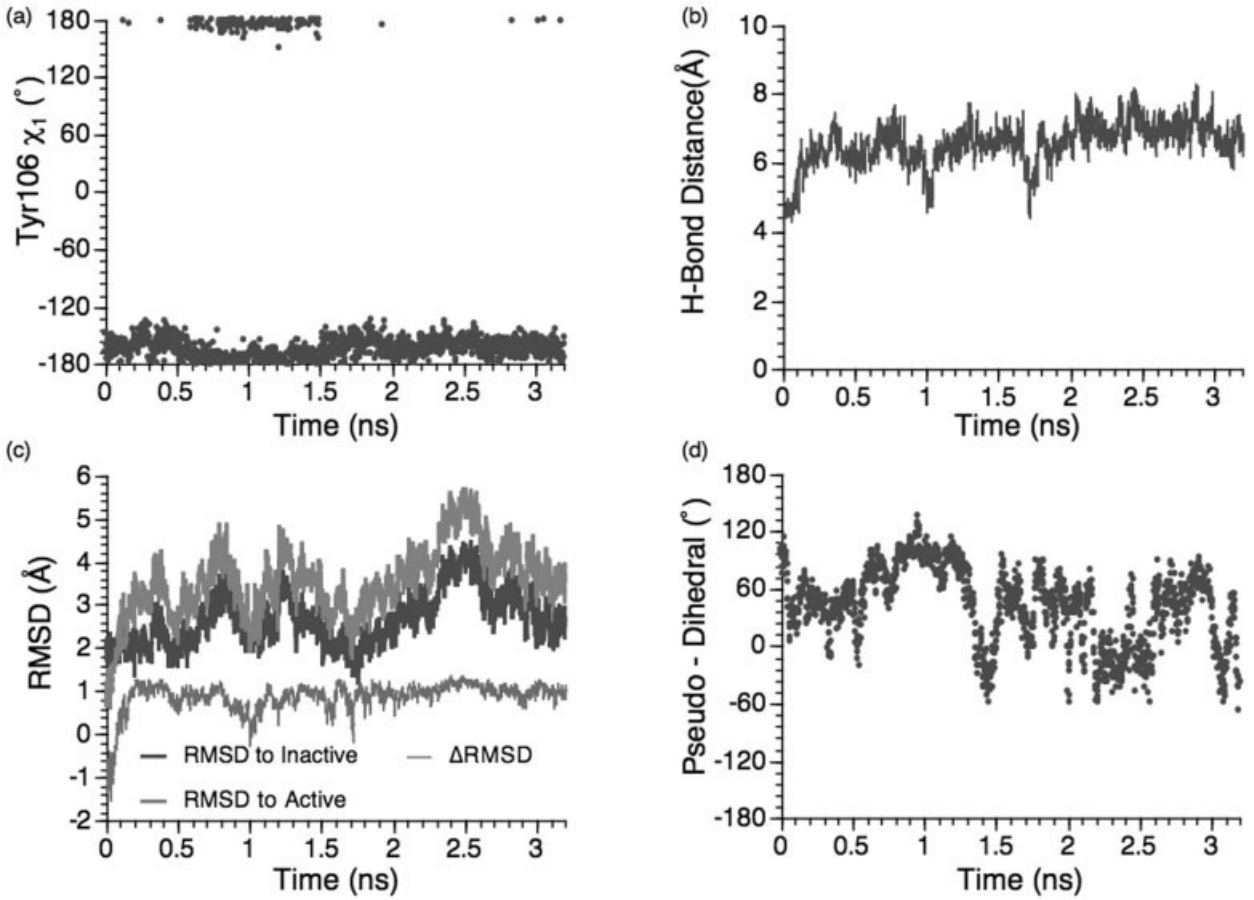

Fig. 9. Key properties during one unbiased explicit solvent simulation of the phosphorylated-active state of the T87A mutant (Set 7 in Table I). See Figure 2 caption for notations. Note the spontaneous β4–α4 loop transition toward the inactive configuration, as reflected by the ΔRMSD, which was not found in the wild-type simulations (Fig. 3).

Coupling between the β4–α4 loop and Tyr 106 rotation

The coupling between the β4–α4 loop and Tyr106 rotation was more difficult to show in an unbiased fashion via simulation due to the slow time scale of *both* events. Carefully designed biased simulations, nevertheless, strongly suggest the coupling between them. Biasing the loop from the inactive toward the active configurations led to *spontaneous* isomerization of Tyr106 in two out of seven simulations. The fact that driving the loop did not induce Tyr106 rotation in all simulations was not surprising, because such rotation likely has a barrier at least comparable to k_BT even in the absence of any interaction with the doorway residues or the β4–α4 loop; it was actually striking that rotation of Tyr106 was observed in simulations where only the loop was biased. In a set of biased simulations (data not included) of a related response regulator, FixJ, the same protocol induced isomerization of the Tyr106 equivalent (Phe101 in FixJ) in all simulations (five were carried out). Analysis of the trajectories suggests that the tighter coupling between loop transition and ring rotation in FixJ is likely due to the larger-scale loop displacement (all-non-hydrogen RMSD between the inactive/active loop configuration is 3.6 Å and 5.5 Å in CheY and FixJ, respectively); as a result, biasing the loop in FixJ created a cavity with a wider "doorway" at the buried site, which makes the transition of Phe101 very facile.

When the rotation of Tyr106 was biased, the response of the β4–α4 loop due to the steric interaction with Ala90 was apparent. Since Asp57 was not phosphorylated, only a partial loop transition was observed after Tyr106 adopted the buried position; this is actually consistent with the meta-active X-ray structure,[37] and further supports the role of Thr87 in stabilizing the active loop configuration (Thr87 remained in the inactive position in these simulations).

Experimental evidence

The mechanism based on the β4–α4 loop is consistent with all available experimental data regarding the activation of CheY. The importance of Thr87 in stabilizing the active configuration of the (at least partially) gating β4–α4 loop provides an alternative explanation (in contrast to the "Y–T" coupling scheme) why Thr87 is a conserved residue in many response regulator proteins, such as CheY, FixJ, and Spo0. In the absence of Thr87, due to the presence of NH of Ala88, however, we anticipate that the loop still has a non-negligible population in the active configuration

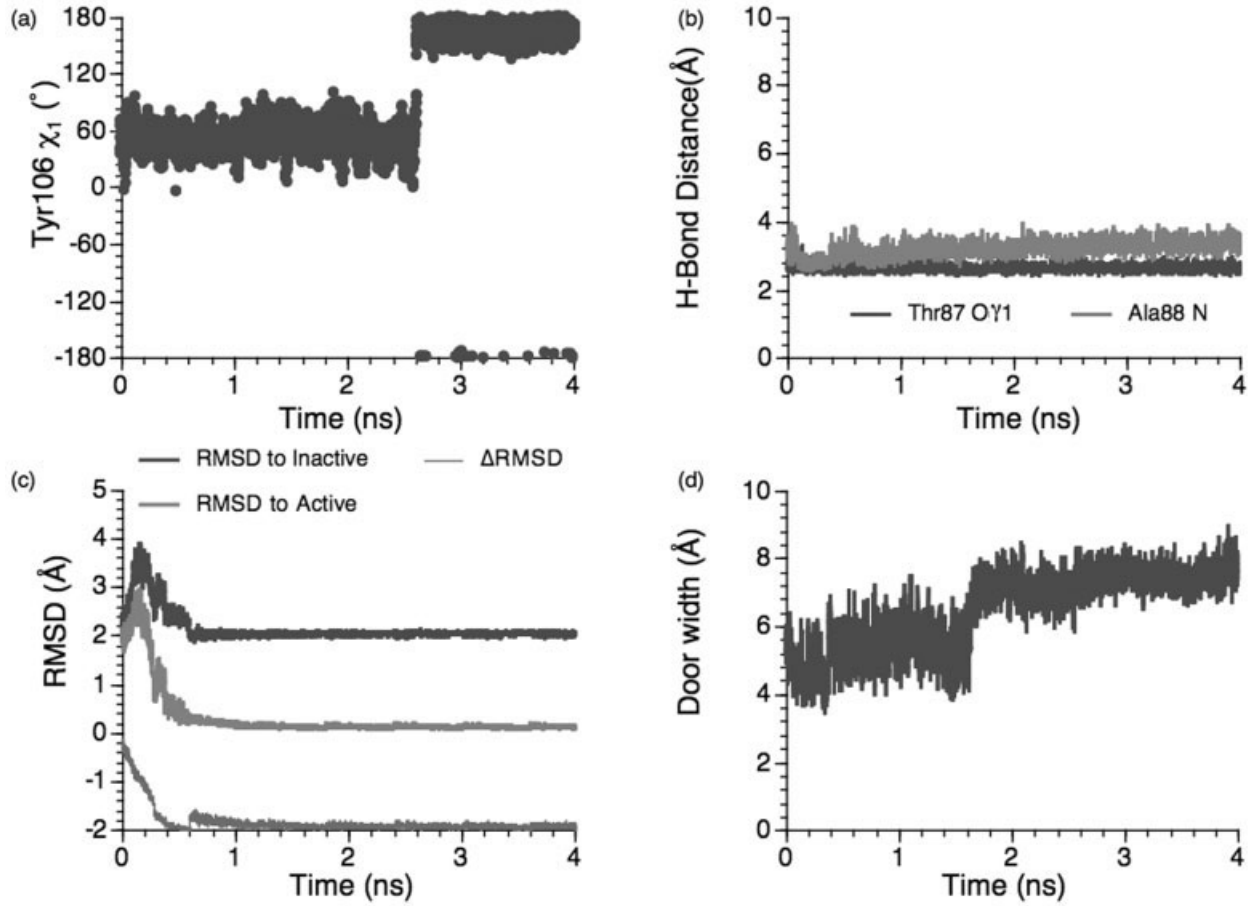

Fig. 10. Key properties during one BMD simulation in which the β4–α4 loop was driven from the inactive to the active configuration. The simulation started from a snapshot in the phosphorylated-inactive state using the implicit solvent model. See Figure 2 caption for notations in (**a**)–(**c**). In (**d**), the size of the doorway formed by Ile95 and Val108 (as measured by the minimal distance between non-hydrogen atoms in those two residues) during the simulation is shown.

when Asp57 is phosphorylated, which explains the observation of partial activity for T87 mutants and that of T87S having a higher activity than T87A (Ser has a OH group capable of hydrogen-bonding to the phosphate).[51] By a similar argument, it is comprehensible that partial activity was observed for wild-type CheY in the absence of phosphorylation. In fact, as mentioned above, the model is consistent with all features of the "meta-active" X-ray structure[37]: Transition of the β4–α4 loop toward the active configuration allows Tyr106 to adopt the buried position, while the absence of phosphate leaves Thr87 and the loop predominantly in the inactive configuration.

The proposal that the β4–α4 loop is at least partially gating is consistent with the result of the A90V mutation, which showed that FliM binding was greatly reduced[64] and flagella rotated CCW (though some wild-type swarming behavior was observed).[65] The role of Val108 and Ile95 as the doorway residues, as observed in the biased MD simulations, is consistent with the mutation data related to these residues, although it is not always straightforward to interpret phenotype observations due to the involvement of other proteins in the chemotaxis signaling network. The V108M mutation showed similar results as the A90V study, confirming that Val108 does play an important role. Substituting Ile95 with the smaller valine produced an overactive (tumbly) phenotype with enhanced binding affinity of FliM[66]; mutations to a bulky group (Met) and charged groups (Asp and Lys), on the other hand, showed impaired signaling.[67] In the unphosphorylated I95V crystal structure,[67] both "in" and "out" positions were occupied, although the electron density for the "in" position was not well resolved. Mutating Ile95 into Ala produced results more complicated to interpret; the rotational bias of the flagella was similar to that in the wild-type, though FliM binding was reduced.[67] The cocrystal of activated CheY with $FliM_{16}$ peptide reveals that Ile95 interacts with three nonpolar (Leu) residues on $FliM_{16}$.[38] The CheZ–CheY cocrystal also shows this interaction between Ile95 and three Leu residues on the C-terminal of CheZ.[68] Therefore, the I95A mutation allowed CheY to remain in the phosphorylated state longer (due to reduced binding to CheZ), thus producing similar flagella behavior despite reduced FliM binding.

Another site that has attracted attention is Lys109, which forms a hydrogen bond with the phosphorylation site; the backbone of Lys109 also forms a hydrogen bond with that of

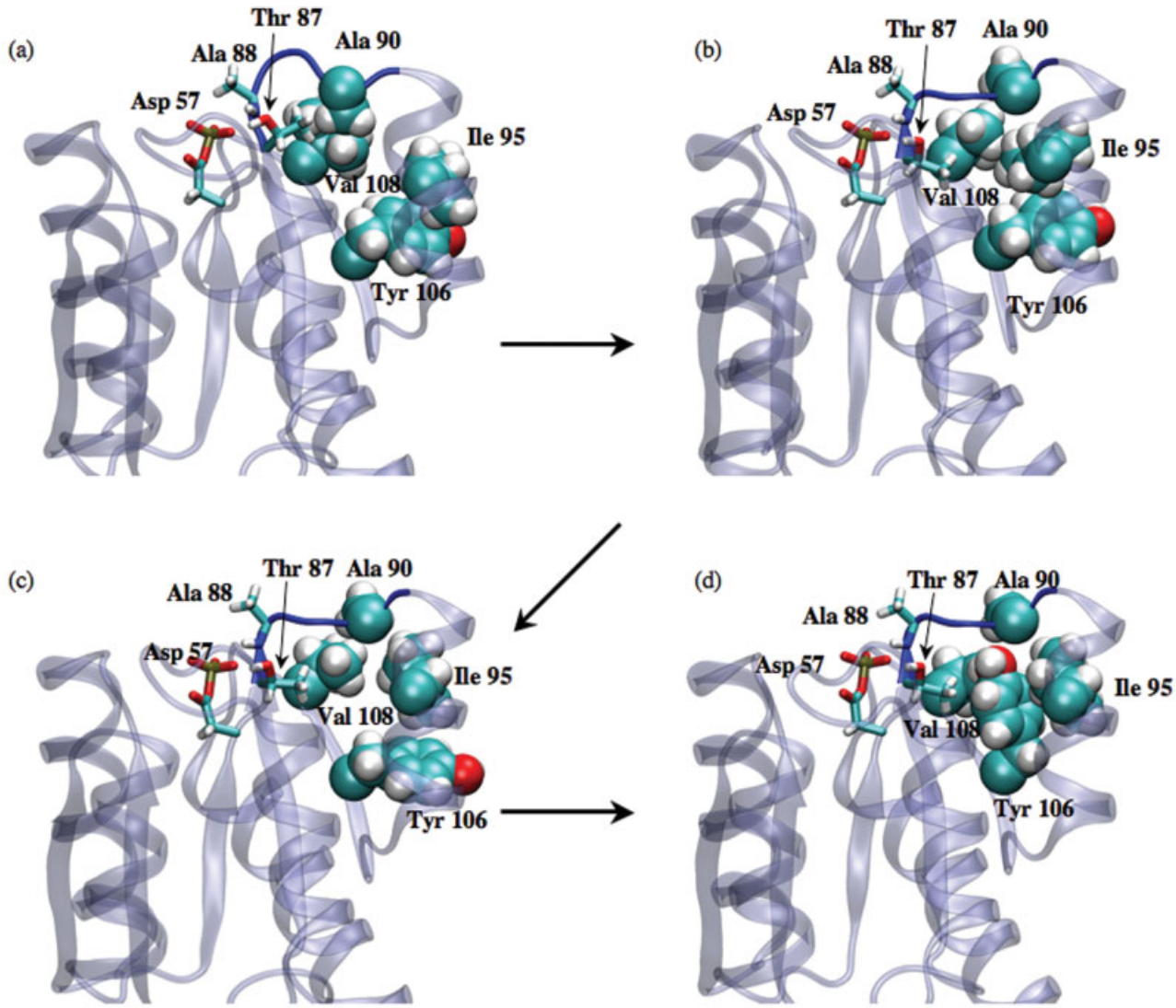

Fig. 11. Snapshots from the loop-driven BMD simulation at 0.0, 1.8, 2.4, and 6.8 ns. Note that after Ala90 is displaced (**b**), the doorway formed by Ile95 and Val108 remains too narrow to allow the transition of Tyr106 into the buried site. [Color figure can be viewed in the online issue, which is available at http:///www.interscience. wiley.com.]

Thr87. Those structural features led to the proposal that Lys109 might be involved in the activation process, although the mechanism was not clear.[69] The mutation of Lys109 into Arg did not affect phosphorylation,[70] yet FliM binding and subsquent rotation of the flagella was modified.[71] The precise role of Lys109 was not transparent from the current simulation, although it was interesting to note that the hydrogen bond between Lys109 and Asp57 was most stable *only* in the phosphorylated active simulations; rather frequent breaks in this interaction were observed in all other states (data not shown). Therefore, it is plausible that Lys109 participates in orienting the phosphate group in the active conformation of the protein, thus playing an indirect role in the activation process.

Reconciling the "old" and "new" Views

How does our study fit into the analysis of the "old" (induced fit)[8–10] and "new" (population shift)[25,26] views of allosteric transitions in general? As summarized in the Introduction, the major differences between the two views apparently concern (1) whether the activated conformation is significantly populated prior to the activation event, and (2) whether there is a well-defined structural pathway(s) that connects the activation and activated sites. Using CheY as a specific example, the traditional "Y–T" coupling scheme involves a sequence of ordered events through steric interactions and is rem-iniscent of the induced fit view. The experimental observation that partial chemotaxis activity (assumed to be directly correlated with the Tyr106 rotation[38,40,42]) exists in the absence of phosphorylation[50] and the "meta-active" X-ray structure[37] all seem to support the population shift model, which implies that the role of phosphorylation is to shift the pre-existing equilibrium between the solvent-exposed and buried conformations of Tyr106 toward the latter.

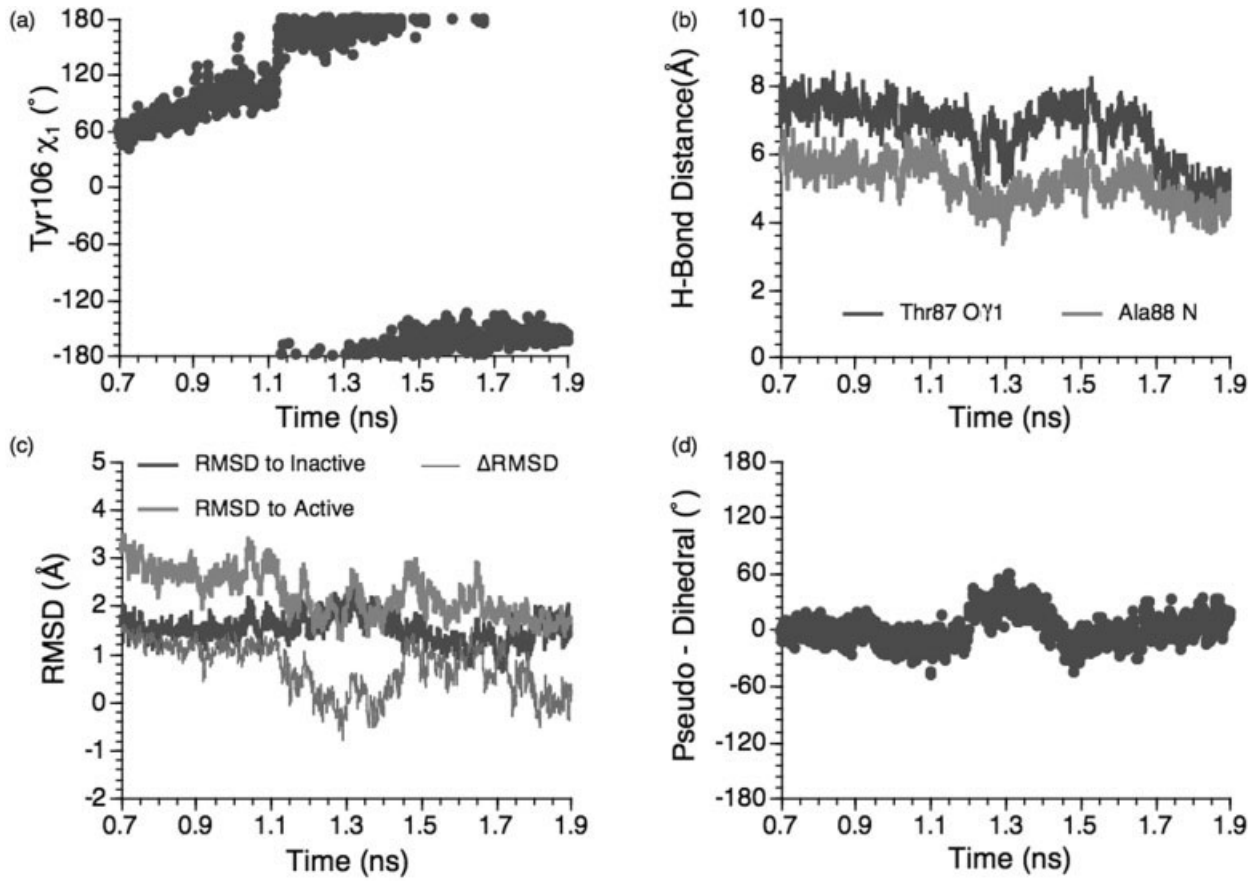

Fig. 12. Key properties during one BMD simulation in which the Tyr106 side-chain was driven from the inactive (solvent-exposed, "out") to the active (buried, "in") configuration. The simulation started from a snapshot in the unphosphorylated-inactive state using the implicit solvent model. See Figure 2 caption for notations. Note the change in ΔRMSD and the pseudodihedral angle when Tyr106 makes the transition (~1.1 ns).

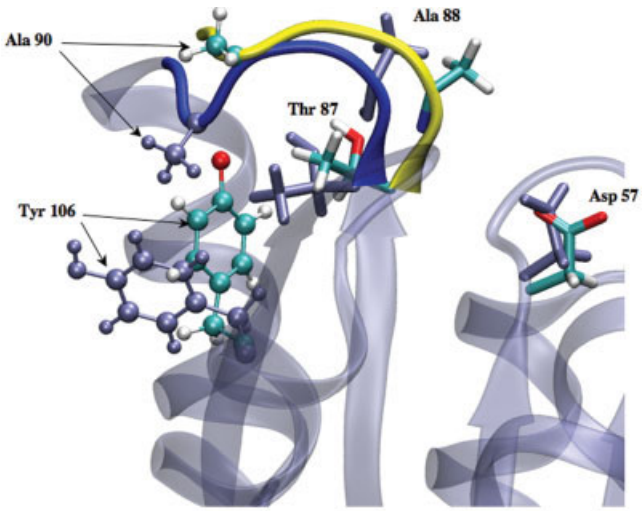

Fig. 13. Overlay of snapshots from the Tyr106-driven BMD simulation to illustrate the response of the β4–α4 loop to the transition of Tyr106 (~1.1 ns). Color coding is the same as in Fig. 1. Residues adopting active-like configurations are color-coded based on atom types, and those adopting inactive-like configurations are colored ice-blue; the active-(inactive-)like loop configuration is dark-blue (yellow). [Color figure can be viewed in the online issue, which is available at http:///www.interscience.wiley.com.]

TABLE II. Estimated Binding Free Energy (kcal/mol) of the Tyr106 Side-Chain to the Rest of the CheY Protein[a]

Asp57 chemical state[b]	Conformation[b]	Tyr106[b]	ΔE_{elec}	ΔE_{vdW}	ΔG_{bind}^{LRA}
UnP	Inactive	Out	−12.6	−12.6	−6.9
P	Active	Out	−12.4	−12.6	−6.9
P	Active	In	−9.2	−15.2	−6.1 + γ
UnP	Meta-active	In	−8.6	−16.2	−6.1 + γ

[a]A linear response model[54] based on the interaction between the Tyr106 side-chain and the environment (ΔE_{elec}, ΔE_{vdW}) was used. See Computational Methods section for details.
[b]See footnotes in Table I for notations.

Although results from this work did not support the traditional "Y–T" coupling scheme and provide an alternative explanation for the conservation of Thr87 in CheY and related response regulator proteins,[59] the endorsed mechanism,[37] in fact, has flavors of both the "old" and "new" views. On the one hand, this mechanism proposes that the roles of phosphorylation and Thr87 are to stabilize the active configuration of the β4–α4 loop, which was shown explicitly by the current simulations to play an important

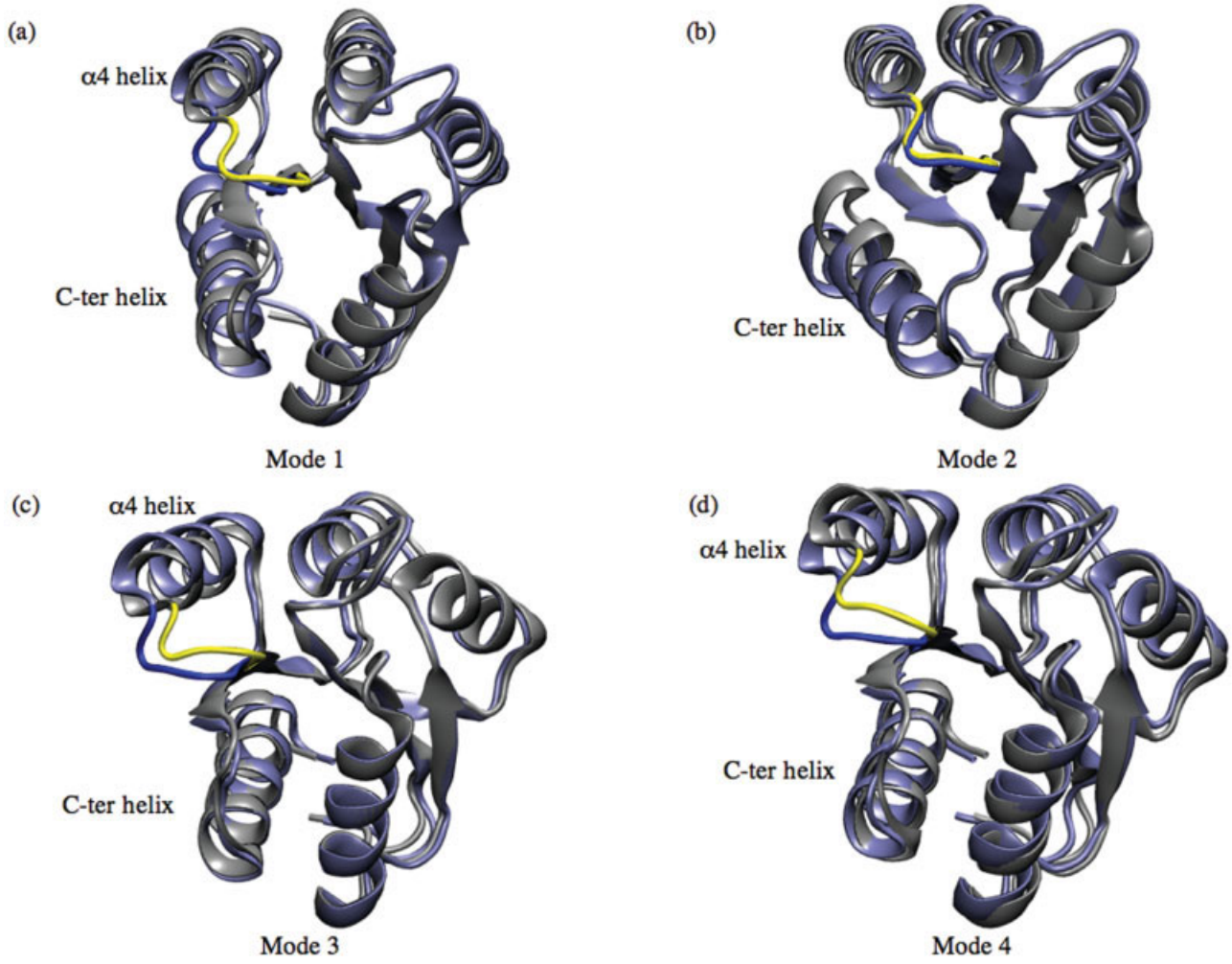

Fig. 14. Character of the first four low-frequency modes illustrated by the overlay of end-structures sampled along the corresponding eigenvectors at 3000 K. [Color figure can be viewed in the online issue, which is available at http:///www.interscience. wiley.com.]

regulatory role in the rotation of Tyr106. In other words, it is envisioned that the gating loop is in equilibrium between the inactive and active(-like) configurations even in the absence of phosphorylation or Thr87 in certain mutants. Their presence, however, shifts the dominant loop population toward the active configuration, in line with the "new" view. The current work also has facets of the "old" view in that it highlights a coupling pathway going from the phosphorylation site through the β4–α4 loop, and to the final activation site of Tyr106. An important distinction, however, is that the mechanism does not specify the sequence of events (e.g., phosphorylation may occur after the loop transition during the activation of a single CheY molecule).

Fitting the CheY activation mechanism into the framework of "old" and "new" views therefore help to better compare the two viewpoints and expose their limitations. The "old" view[8–10] emphasizes that there is a set of well-defined residues and interactions that couple events at two distant sites in a "domino" fashion. This is sensible because "hot spot" residues have been identified in many allostery systems.[11–18] However, the limitation of the induced fit view is that it often envisions a highly ordered sequence of events (literally, domino propagation) that may lead to incorrect mechanistic interpretation for the roles of conserved or "hot spot" residues; the way "Y–T" coupling describes CheY activation and rationalizes the role of Thr87 is an excellent example.

The "new" view invokes population shift and often refers to changes of the entire energy landscape once the system is modified by the activation event. This "energy landscape" view does not emphasize sequence of events per se; in fact, proponents of the population shift view often argue for the occurrence of the the activated event (e.g., conformational change at the response site) prior to the activation event (e.g., phosphorylation).[25,26] Observing an experimental signature[23,22] of the activated conformation in the absence of activation was an impressive achievement and prompted us to be cautious about causality assumed in the traditional "domino" view. However, as a general mechanism, it is difficult to establish a nonarbitrary threshold for a "pre-existing" population; any conformation has a

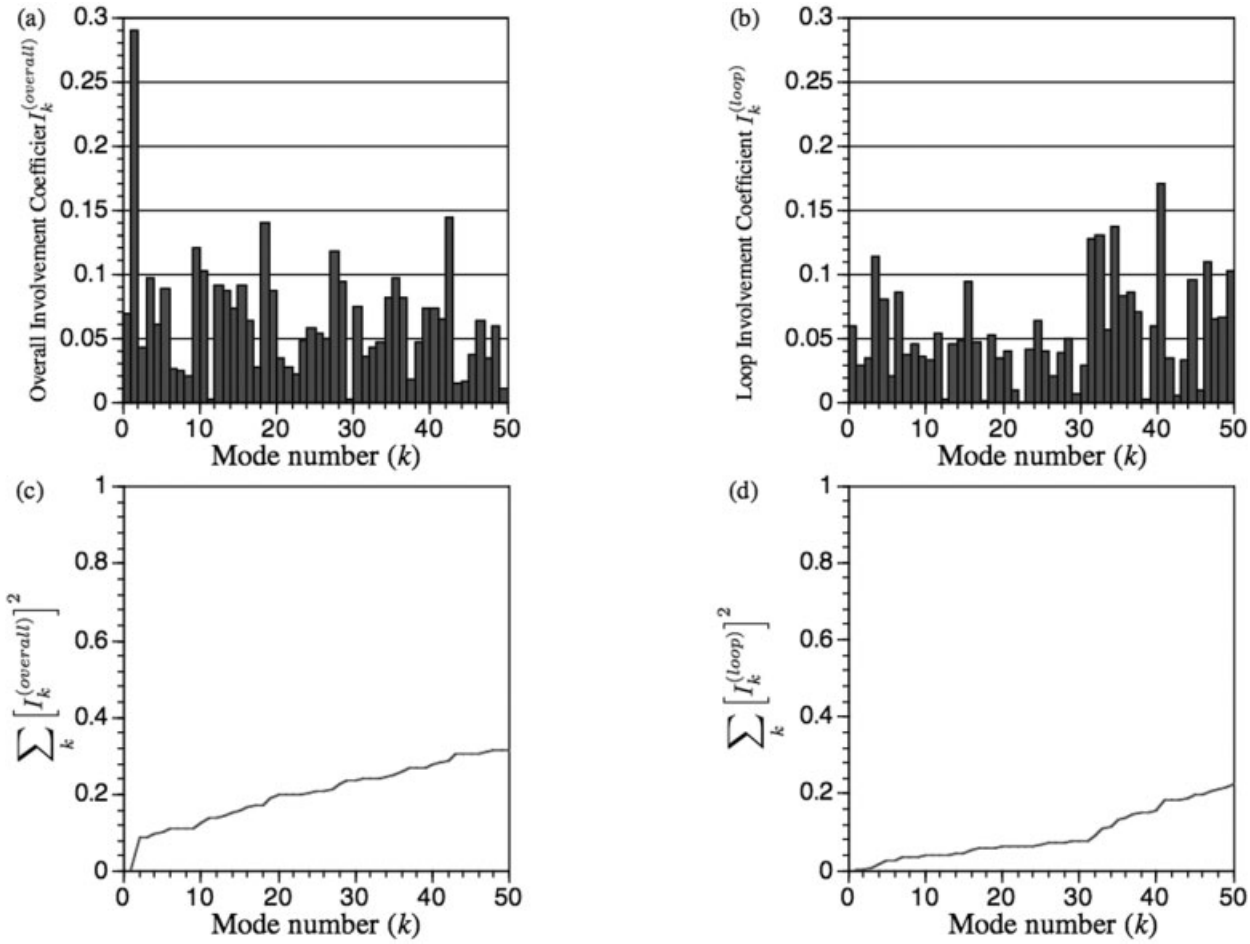

Fig. 15. Involvement coefficients for the low-frequency modes of CheY based on the minimized unphosphorylated-inactive structure, its normal modes, and the X-ray structure for the active state: (**a**) the overall involvement coefficients; (**b**) the local involvement coefficients for the β4–α4 loop only; and the (**c**) cumulative overall and (**d**) loop involvement coefficients.

nonzero population under any condition (though not necessarily detectable using a specific experimental technique), which seems to make the population shift model "trivially" true.

More importantly, the limitation of invoking merely "population-shift," which is a thermodynamic argument, is that it offers little explicit mechanistic insight into two key questions:

1. How does the system acquire the intrinsic structural flexibility such that a significant population of the activated conformation exists prior to the activation event?
2. *How* is population shift achieved by the activation event?

Regarding the first issue, although possessing inherent structural flexibility for molecules whose function involves substantial conformational transitions makes perfect biological sense, it is of interest to inquire how such functional flexibility is acquired. A similar comparison can be made to enzymes, in which the chemical event can often become non-rate-limiting[72]; this does not make it uninteresting to study the chemical mechanism in these enzymes. In fact, the interesting question is precisely how these enzymes can speed up chemistry by so much. Regarding the second issue, we consider rationalizing allosteric transition via change in the entire energy landscape incomplete reasoning, because the heart of the question *is* about how a local activation event can cause substantial change in the energy landscape such that the property (e.g., conformation) of a distant site is affected. This argument does not invalidate algorithms based on the "redistribution of conformational ensemble" framework,[26–28,30] but only highlights the need to better understand why such algorithms work well. Similarly, explaining population shift in terms of stabilized conformation via interactions localized to the activation site is also incomplete, because including only two populations in the discussion implicitly *assumes* that configurations of the activation site and the response site are tightly coupled (thus, stabilizing a specific configuration of the activation site will automatically stabilize the activated configuration of the response site), which is precisely the phenomenon that needs to be explained (see

next subsection). In CheY, for example, it would be incomplete to rationalize Tyr106 rotation by the stabilizing hydrogen bonding between Thr87 and the phosphate, without explaining how such an interaction modulates the configuration of the β4–α4 loop, which, in turn, regulates the rotation of Tyr106.

Therefore, it is clear that neither the induced fit nor the population shift view is complete. In our opinion, the fundamental conflict between the two frameworks of thinking arises largely due to the different points of emphasis; the induced fit view attempted to emphasize the coupling mechanism between two distant sites *during* the transition, while the population shift view emphasizes the structure–thermodynamics relation of the system in the *end states.* In other words, the induced fit view is kinetics-driven, while the population shift view is thermodynamics-driven. A *generally* valid mechanistic picture, if it exists, should reconcile the two by combining their features, because both kinetic and thermodynamics aspects need to be addressed for a complete understanding.[73] Alternatively speaking, both kinetics and thermodynamics are determined by the free energy landscape of the system; thus, a complete understanding requires detailed analysis of the free energy surface before and after the activation event, as we attempted to do at a qualitative level for CheY.

Collective Motion and Allostery

Finally, we briefly consider, collective motion in biomolecules as a possible general cause of allostery. An emerging theme from the studies of a number of enzymes[74–76] and large molecular assemblies[77,78] is that *intrinsic* long-range motion correlation is present in those systems as reflected by, for example, collective low-frequency modes[55–57] or the displacement covariance matrix.[76] Therefore, perturbing one site (e.g., by ligand binding) will likely affect a distant site to which it is significantly correlated,[74,79] which seems to be a logical mechanism for "population shift" and therefore an explanation of allostery.[25,80,81] We note that compared to the traditional induced fit model, the description involving collective motion replaces the *sequential* local conformational propagation by *concerted* collective transition as the mechanism for coupling changes at distant sites (also see below). There are a number of other considerations that make it attractive to relate collective motion (modes) to allostery. First, notable displacement along collective modes is plausible even in the absence of the activation event, which is consistent with the pre-existing activated(-like) population detected experimentally in several systems.[23,25] Second, long-range correlation is determined largely by the shape and mass distribution of the system, as are low-frequency modes of large biomolecules, although other factors, such as solvent motion, may play a role.[82–85] Therefore, involving collective motion to implement allostery is likely robust from the evolutionary point of view. Finally, it is still possible to rationalize the existence of "hot spot" residues, which are likely the hinge residues in important collective modes. For example, hinge residues identified by normal mode analysis in the molecular motor myosin[56,86] were found to be crucial to the mechanochemical coupling; mutation of these residues abolished the coupling between motility and ATPase activity.[13,14]

Despite those favorable considerations, however, we caution that the usefulness of dissecting allosteric transition based on collective modes is likely system-dependent. In CheY, for example, the proposed gating loop and the conserved Thr87 do not exhibit any distinct signature in low-frequency modes. Even in systems where low-frequency modes were found to correlate well with observed structural changes,[55–57,80,81] care must be taken not to overinterpret the correlation. In the aforementioned myosin, for example, a number of residues known to be important to the mechanochemical coupling (e.g., Gly457) were difficult to identify based on normal mode analysis; this is not surprising, because normal mode analysis is an equilibrium technique in nature, and some residues can be identified only with algorithms that explicitly sample the ki netics of the transition process.[87–90] In other words, the allosteric transition may involve both concerted collective motions and sequential local structural distortions, and it is entirely possible that displacements along collective modes do not, in fact, constitute the kinetic bottleneck. In DNA polymerase, for example, it was argued that side-chain isomerization, rather than large-scale domain motion, dictates the kinetics.[89] In a "protein-quake" model,[90] local unfolding makes an important contribution to the activation free energy for the allosteric transition, although the model used was rather approximate. In the future, it is of interest to develop intermediate-resolution molecular models that allow unbiased simulation of allosteric processes, so that the interplay between concerted collective motion and sequential local structural changes in realistic systems can be better clarified.[73,91] On the other hand, we note that mutations may affect allosteric transitions by modifying the rate-limiting step; this is why residues important for functionally relevant collective motions are likely conserved even if displacements along such modes are not rate limiting in the wild-type system.

CONCLUSION

Motivated by better comparison of the "old" (induced fit) and "new" (population shift) views of allosteric transitions in biomolecules, we chose a small signal transduction protein, CheY, as a model to study the coupling between two sites separated by ~10 Å. A set of carefully designed simulations was carried out to probe the structural, dynamical, and energetical properties of CheY as a function of the phosphorylation state, in ways more thorough compared to previous explorative simulation of a related response regulator.[53] The sim ulation results and available experimental data can be best interpreted in terms of an alternative mechanism for activation that differs from the widely accepted "Y–T" coupling scheme. This mechanism[37] involves the β4–α4 loop as the gating element, and characterizes the role of phosphorylation and the conserved Thr87 as indirect, in that they regulate the population of the active loop configuration. A set of "doorway"

residues close to the Tyr106 transition site were also identified to potentially contribute to the kinetics of the activation event. This activation mechanism may apply to other response regulators in two component systems. The indirect role of the activation event and/or conserved residues in stabilizing, rather than causing, specific conformational transition is likely a feature found in many signaling systems.

The current study of CheY activation helped to make clear that neither the induced fit nor the population shift view of allosteric transition is complete, because, in our opinion, the essential difference between them is that the two views emphasize kinetic and thermodynamic aspects of the allosteric process, respectively. In other words, the population shift model emphasizes the intrinsic structural flexibility of the biomolecule and the thermodynamical consequence of the activation event but does not readily explain factors responsible for the shift in the population; involving the inactive and activated conformations as the only relevant populations also *implicitly assumes* coupling between the activation and response sites. The induced fit model emphasizes the existence of structural pathways that couple two distant sites for the kinetics of the allosteric transition, but the traditional presentation tends to overemphasize the order and locality in the sequence of events. A coherent mechanistic picture requires studies that address both kinetics and thermodynamics of the transition process, or equivalently, detailed characterization of the energy landscape prior to and after the activation event, as we attempted to do in a qualitative manner for CheY. In this regard, a key conceptual issue concerns the relative importance of *concerted* collective motion and *sequential* local structural changes in coupling the properties of the activation and response sites. Although this remains difficult at a quantitative level, our study has illustrated that useful mechanistic insight can be obtained by carefully designed molecular simulations, especially when a combination of complementary protocols are used. Such studies will ultimately help the design of strategies to effectively regulate allosteric process in important biological and biomedical applications.

COMPUTATIONAL METHODS

Although the conformational transitions involved in CheY are rather subtle compared to typical allosteric systems,[6,7] it is difficult to observe all those transitions in the nanosecond [between 10 ns up to a single 100 ns with the GBSW[92] implicit solvent model) simulations. The transitions are sufficiently complex in nature that it is not straightforward (although several attempts were made) to select a few degrees of freedom to perform meaningful potential of mean force simulations. Therefore, the approach adapted here is to use a number of different types of MD simulations as "computational probes" to deduce factors that dictate the transitions in CheY. All the MD simulations were performed at 300 K with a modified version of CHARMM[93] and the CHARMM22 force field for proteins.[94] These were supplemented by normal mode analysis, which is an alternative way to probe structurally mobile regions in a protein; the calculations were performed with the polar hydrogen parameter set of the CHARMM force field.[95]

Unbiased Molecular Dynamics Simulations

The first set of MD simulations was carried out without any artificial constraints. Five different conditions were studied with the wild type *Escherichia coli* CheY with different combinations of the phosphorylation state of Asp57 and the starting conformation; consistent with the X-ray studies, the three types of conformations, referred to as "inactive,"[37] "active,"[38] and "meta-active,"[37] essentially measure the rotameric state of Tyr106 and the configuration of the β4–α4 loop (see Table I for a summary). Both explicit solvent (TIP3P)[96] and implicit solvent (GBSW[92]) simulations were carried out for each condition, and multiple runs were carried out for each combination of condition and solvent model (for details, see Supplementary Materials). Typically 10 ns simulations were carried out for both explicit and implicit solvent simulations, although it is understood that conformational transitions of solvent-exposed residues are likely faster in the implicit solvent simulations due to the neglect of explicit collision with the solvent molecules[60]; the latter was approximated by a Langevin bath with an uniform friction constant of 25 ps^{-1} applied to all non-hydrogen atoms. As discussed above and in a separate publication (Formaneck et al., manuscript in preparation), the explicit and GBSW solvent simulations are, overall, consistent in terms of structural and dynamical properties of CheY, although there are systematic differences that suggest overestimated hydrogen-bonding interactions involving solvent-exposed ionic groups in, the GBSW model (see Discussion section).

To better understand the role of Thr87, a set of unbiased MD simulations was carried out for the T87A mutant. Only the phosphorylated chemical state was studied, starting from appropriately modified (the side-chain of Thr87 was truncated into a methyl group) "inactive" and "active" X-ray coordinates for the wild-type CheY.

Biased Molecular Dynamics (BMD) Simulations

No spontaneous transition of the Tyr106 rotameric state was observed in any of the unbiased MD simulations (between ~10 ns up to a single 100 ns GBSW simulation). Therefore, additional sets of MD simulations were carried out in which specific bias was applied. Although subjecting the entire protein to bias will ensure the observation of the expected transitions during the simulation, the fact that the time scale of the transition has been increased dramatically means that the sequence of events may be altered. Therefore, we chose to bias only a specific part of the protein as a way to probe the coupling (not the precise sequence of events) between different structural motifs. One important element is the β4–α4 loop. Other than the fact that this loop undergoes substantial changes from the inactive to phosphorylated (BeF_3^-) active structures [Fig. 1(a)], it was suspected[37] that the β4–α4 loop may function as an important gating element, because the side-chain of Ala90 in the inactive loop is in a position that blocks the

rotation of Tyr106 [Fig. 1(b)]; in the active loop configuration, by contrast, Ala90 points away and thus conceivably leaves more room for Tyr106 to undergo isomerization. Thus, the first set of BMD simulations biased the β4–α4 loop from the inactive to the active configurations in the respective X-ray structures. The second set of biased simulations drove the isomerization of the Tyr106 side-chain explicitly, and the response from the nearby structural motifs was monitored. The biasing coordinate in the early stage of the BMD simulations was the differential RMSD between the coordinate at time t relative to the "inactive" and "active" X-ray coordinates,

$$\Delta\mathrm{RMSD}[\mathrm{X}(t)] = \mathrm{RMSD}[\mathrm{X}(t);\mathrm{active}] - \mathrm{RMSD}[\mathrm{X}(t);\mathrm{inactive}]\,, \quad (1)$$

where RMSDs were measured for the biased degrees of freedom only, which involved only the non-hydrogen atoms in either the β4–α4 loop or the Tyr106 side-chain. Note that the reference (inactive, active X-ray) structures need to be constantly (every 5 MD steps) best-fit to the running structure based on *all backbone atoms,* because the running structure undergoes overall rotation during the BMD simulation (Formaneck, Cui, unpublished data). The ΔRMSD[X(t)] was controlled in the BMD simulations via a harmonic constraint whose constraining center was monotonically decreased between appropriate values [(±ΔRMSD(inactive, active)] at a rate consistent with the length of the simulation; the force constant of the constraint was chosen to be ~1000 kcal/(mol · Å^2). Even for Tyr106, the ΔRMSD coordinate was found to be more useful than a simple side-chain dihedral angle (χ_1), highlighting the complexity of the isomerization in a protein environment. In the late stage of the BMD simulations, it was useful to switch to a biasing coordinate that depends only on the RMSD with respect to the final target (active) conformation; the switch from ΔRMSD to a single RMSD was made after about 1.8 ns for the loop-driven simulations, and after 600 ps for the Tyr106-driven simulations. Multiple sets of BMD simulations were carried out, and all simulations used the GBSW implicit solvation model. All BMD simulations started from equilibrated, unbiased simulations of the X-ray inactive structure,[37] al though the phosphorylated and unphosphorylated chemical state was chosen for Asp57 in the loop-driven and Tyr106-driven simulations, respectively.

To further corroborate the trends seen in CheY, a set of BMD simulations was carried out for a related response regulator, FixJ, a protein involved in nitrogen fixation in bacteria.[48] The results are qualitatively similar to the previous study[53] and have therefore not been included. It was interesting to note that the hydrogen-bonding interaction between the Thr and phosphate always formed *prior to* the transition of Phe101 (the equivalence of Tyr106) in our biased simulations, in contrast to the previous work; the discrepancy is likely due to the difference in the simulation protocol (Roche et al.[53] carried out vacuum simulations). Although Roche et al. used this as a piece of evidence to support the population shift view of FixJ activation, we believe this is less important compared to establishing the role of the β4–α4 loop in regulating the Phe101 rotation.

Binding Free Energy of Tyr106

To better characterize the interaction between Tyr106 and the protein, the "binding free energy" between the Tyr106 side-chain and the rest of the protein in different conformational states was analyzed in the framework of a linear response model.[54] Using configurations collected from the unbiased simulations with the explicit solvent model, the average electrostatic (elec) and van der Waals (vdW) interactions between the Tyr106 side chain and rest of the protein/solvent atoms were calculated. These components were then scaled by the appropriate factors to estimate a binding free energy of Tyr106 side chain to different CheY conformations,[97]

$$\Delta G_{bind} = \alpha\langle\Delta E_{vdW}\rangle + \beta\langle\Delta E_{elec}\rangle + \gamma\,, \quad (2)$$

where $\alpha = 0.18$,[97] $\beta = 0.37$.[100] The choice for the value of γ is more complicated, as discussed in a recent study.[97] It was found that the appropriate value depends on the hydrophobicity of the binding site. For a polar binding pocket, $\gamma = 0$ kcal/mol works well; this is used for estimating the binding of Tyr106 to the "out" position. For the most hydrophobic pocket tested, however, a value of −7.0 kcal/mol was found to give the best fit to experimental measured binding affinities.[97] Although this value could be adopted for the "in" position here, we note that γ cancels out for the *relative* binding free energy with different protein conformations ("meta-active" vs "active"). Therefore, γ was simply included as a variable in the reported binding free energies to the "in" position in Table II. We emphasize that the linear response model is not as rigorous as explicit free energy perturbation calculations. However, its simplicity is a desired feature for the current purpose of analyzing interactions between the protein and Tyr106 at different conformations.

Normal Mode Analysis (NMA)

To characterize the intrinsic structural flexibility of CheY, normal mode analysis was performed for the inactive-unphosphorylated state of CheY. As discussed extensively in previous studies,[55–57] the NMA results complement more detailed MD simulations in that no explicit time scale limitation applies. The NMA was performed using the standard procedure in CHARMM.[93] The x-ray structure[37] was first minimized using the CHARMM19 polar-hydrogen force field[95] in vacuum; partial charges of charged side-chains were scaled by an empirical factor of 0.3.[55] Test calculations were also performed using the EEF1 implicit solvent model,[98] which gave very similar results. The final gradient after minimization was 6×10^{-5} kcal/(mol · Å), and all-non-hydrogen RMSD relative to the X-ray structure was 1.53 Å.

To characterize the relevance of the low-frequency modes to the observed structural transitions, involvement coefficients[99] were computed for both the overall structural change and the β4–α4 loop transition:

$$I_k^{(\text{overall})} = \frac{\mathbf{X}_{min}(\text{inactive}) - \mathbf{X}_{X\text{-}ray}(\text{active})}{|\mathbf{X}_{min}(\text{inactive}) - \mathbf{X}_{X\text{-}ray}(\text{active})|} \cdot \mathbf{L}_k \quad (3)$$

$$I_k^{(\text{loop})} = \frac{\mathbf{X}_{min}{}^{loop}(\text{inactive}) - \mathbf{X}_{X\text{-}ray}{}^{loop}(\text{active})}{|\mathbf{X}_{min}{}^{loop}(\text{inactive}) - \mathbf{X}_{X\text{-}ray}{}^{loop}(\text{active})|} \cdot \mathbf{L}_k , \quad (4)$$

where $\mathbf{X}_{min}$(inactive) and $\mathbf{X}_{X\text{-}ray}$(active) are the Cartesian coordinates for the minimized inactive conformation[37] and X-ray active conformation,[38] respectively; $\mathbf{L}_k$ is the kth eigenvector computed for the inactive structure. In addition, the cumulative involvement coefficients were computed, which reflect the degree of conformational transition covered by up to k modes, for example, $\Sigma_{j=1}^{k} [I_j^{(loop)}]^2$, starting from the lowest-frequency mode ($k = 1$).

ACKNOWLEDGMENTS

Computational resources from the National Center for Supercomput-ing Applications at the University of Illinois are greatly appreciated.

REFERENCES

1. Alberts B, Bray D, Lewis J, Raff M, Roberts K, Watson JD. Molecular biology of the cell. Garland; 1994.
2. Monod J, Wyman J, Changeux JP. On the nature of allosteric transitions: a plausible model. J Mol Biol 1965;12:88–118.
3. Koshland DE Jr, Nemethy G, Filmer D. Comparison of experimental binding data and theoretical models in proteins containing subunits. Biochem 1966;5:365–385.
4. Szabo A, Karplus M. A mathematical model for structure–function relations in hemoglobin. J Mol Biol 1972;72:163–197.
5. Cooper A, Dryden D. Allostery without conformational change. Eur Biophy J 1984;11:103–109.
6. Perutz MF. Stereochemistry of cooperative effects in haemoglobin. Nature 1970;228:726–739.
7. Ma J, Sigler PB, Xu Z, Karplus M. A dynamic model for the allosteric mechanism of GroEL. J Mol Biol 2000;302:303–313.
8. Koshland DE. Application of a theory of enzyme specificity to protein synthesis. Proc Natl Acad Sci USA 1958;44:98–104.
9. Ottemann KM, Xiao W, Shin YK, Koshland DEJ. A piston model for transmembrane signaling of the aspartate receptor. Science; 285:1751–1754.
10. Yu EW, Koshland DE Jr. Propagating conformational changes over long (and short) distances in proteins. Proc Natl Acad Sci USA 2001;98:9517–9520.
11. Vanvliet F, Xi XG, Destaercke C, Dewannemaeker B, Jacobs A, Cherfils J, Ladjimi MM, Herve G, Cunin R. Heterotropic interactions in aspartate transcarbamoylase—turning allosteric ATP activation into inhibition as a consequence of a single tyrosine to phenylalanine mutation. Proc Natl Acad Sci USA 1991;88:9180–9183.
12. Pardanani A, Gibson QH, Colotti G, Royer WE. Mutation of residue phe97 to Leu disrupts the central allosteric pathway in *Scapharca* dimeric hemoglobin. J Mol Biol 1997;272:13171–13179.
13. Ito K, Uyeda QP, Suzuki Y, Sutoh K, Yamamoto K. Requirement of domain–domain interaction for conformational change and functional ATP hydrolysis in myosin. J Biol Chem 2003;278: 31049–31057.
14. Sasaki N, Ohkura R, Sutoh K. *Dictyostelium* myosin *ii* mutations that uncouples the converter swing and ATP hydrolysis cycle. Biochemistry 2003;42:90–95.
15. Heidary DK, Roy M, Daumy GO, Cong Y, Jennings PA. Long-range coupling between separate docking sites in interleukin-1β. J Mol Biol 2005;353:1187–1198.
16. Lockless SW, Ranganathan R. Evolutionarily conserved pathways of energetic connectivity in protein families. Science 1999; 286:295–299.
17. Suel GM, Lockless SW, Wall MA, Ranganathan R. Evolutionarily conserved networks of residues mediate allosteric communication in proteins. Nat Struct Biol 2003;10:59–69.
18. Shulman AI, Larson C, Mangelsdorf DJ, Ranganathan R. Structural determinants of allosteric ligand activation in RXR heterodimers. Cell 2004;116:417–429.
19. Clarkson MW, Lee AL. Long-range dynamic effects of point mutations propagate through sidechains in the serine protease inhibitor eglin c. Biochemistry 2004;43:12448–12458.
20. Palmer AG. NMR characterization of the dynamics of biomolecules. Chem Rev 2004;104:3623–3640.
21. Eisenmesser EZ, Bosco DA, Akke M, Kern D. Enzyme dynamics during catalysis. Science 2002;295:1520–1523.
22. Wolft-Watz M, Thai V, Henzler-Wildman K, Hadjipavlou G, Eisenmesser EZ, Kern D. Linkage between dynamics and catalysis in a thermophilic–mesophilic enzyme pair. Nat Struct Mol Biol 2004;11:945–949.
23. Volkman BF, Lipson D, Wemmer DE, Kern D. Two-state allosteric behavior in a single-domain signaling protein. Science 2001; 291:2429–2433.
24. Rueda D, Bokinsky G, Rhodes MM, Rust MJ, Zhuang XW, Walter NG. Single-molecule enzymology of RNA: essential functional groups impact catalysis from a distance. Proc Natl Acad Sci USA 2004;101:10066–10071.
25. Kern D, Zuiderweg ERP. The role of dynamics in allosteric regulation. Curr Opin Struct Biol 2003;13:748–757.
26. Gunasekaran K, Ma B, Nussinov R. Is allostery an intrinsic property of all dynamic proteins? Proteins 2004;57:433–443.
27. Pan H, Lee JC, Hilser VJ. Binding sites in *Escherichia coli* dihydrofolate reductase communicate by modulating the conformational ensemble. Proc Natl Acad Sci USA 2000;97:12020–12025.
28. Hilser VJ, Freire E. Structure-based calculation of the equilibrium folding pathway of proteins: correlation with hydrogen exchange protection factors. J Mol Biol 1996;262:756–772.
29. Hilser VJ, Dowdy D, Oas TG, Freíre E. The structural distribution of cooperative interactions in proteins: analysis of the native state ensemble. Proc Natl Acad Sci USA 1998;95:9903–9908.
30. Whitten ST, Garcia-Moreno B, Hilser VJ. Local conformational fluctuations can modulate the coupling between proton binding and global structural transitions in proteins. Proc Natl Acad Sci USA 2005;102:4282–4287.
31. Blair DF. How bacteria sense and swim. Annu Rev Microbiol 1995;49:489–522.
32. Falke JJ, Bass RB, Butler SL, Chervitz SA, Danielson MA. The two-compenent signaling pathway of bacterial chemotaxis: a molecular view of signal transduction by receptors, kinases, and adaptation enzymes. Annu Rev Cell Dev Biol 1997;13:457–512.
33. Wadhams GH, Armitage JP. Making sense of it all: bacterial chemotaxis. Nat Rev Mol Cell Biol 2004;5:1024–1037.
34. Silversmith RE, Bourret RB. Throwing the switch in bacterial chemotaxis. Trends Microbiol 1999;7:16–22.
35. Djordjevic S, Stock AM. Structural analysis of bacterial chemotaxis proteins: components of a dynamic signaling system. J Struct Biol 1998;124:189–200.
36. Stock A, Robinson V, Goudreau P. Two-component signal transduction. Annu Rev Biochem 2000;69:183–215.
37. Simonovio M, Volz K. A distinct meta-active conformation in the 1.1 Å resolution structure of wild-type apo-CheY. J Biol Chem 2001;276:28637–28640.
38. Lee S-Y, Cho HS, Pelton JG, Yan D, Henderson RK, King DS, Shar Huang L, Kustu S, Berry EA, Wemmer DE. Crystal structure of an activated response regulator bound to its target. Nat Struct Biol 2001;1:52–56.
39. Humphrey W, Dalke A, Schulten K. VMD—visual molecular dynamics. J Mol Graphics 1996;14:33–38.
40. Dyer C, Quillin M, Campos A, Lu J, McEvoy M, Hausrath A, Westbrook E, Matsumura P, Matthews B, Dahlquist F. Structure of the constitutively active double mutant CheY(D13K) Y-106W alone and in complex with a flim peptide. J Mol Biol 2004;342: 1325–1335.
41. Toker AS, Macnab RM. Distinct regions of bacterial flagellar switch protein FliM interact with FliG, FliN and CheY. J Mol Biol 1997;273:623–634.
42. Zhu X, Amsler C, Volz K, Matsumura P. Tyrosine 106 of CheY plays an important role in chemotaxis signal transduction in *Escherichia coli.* J Bacteriol 1996;178:4208–4215.
43. Frauenfelden H, McMahon BH, Austin RH, Chu K, Groves JT. The role of structure, energy landscape, dynamics and allostery in the enzymatic function of myoglobin. Proc Natl Acad Sci USA 2001;98:2370–2374.

44. Rostovtseva TK, Liu TT, Colombini M, Parsegian VA, Bezrukov SM. Positive cooperativity without domains or subunits in a monomeric membrane channel. Proc Natl Acad Sci USA 2000;97: 7819–7822.
45. Volz K. Structural conservation in the CheY superfamily. Biochemistry 1993;32:11741–11753.
46. Cho HS, Lee S-Y, Yan D, Pan X, Parkinson J, Kustu S, Wemmer DE, Pelton JG. NMR structure of activated CheY. J Mol Biol 2000;297:543–551.
47. Lee S-Y, Cho HS, Pelton JG, Yan D, Berry EA, Wemmer DE. Crystal structure of activated CheY. J Biol Chem 2001;276:16425–16431.
48. Birck C, Mourey L, Gouet P, Fabry B, Schumacher J, Rousseau P, Kahn D, Samama J-P. Confromational changes induced by phosphorylation of the FixJ receiver domain. Structure 1999;7: 1505–1515.
49. Lewis RJ, Brannigan JA, Muchová K, Barák I, Wilkinson AJ. Phosphorylated aspartate in the structure of a response regulator protein. J Mol Biol 1999;294:9–15.
50. Barak R, Eisenbach M. Correlation between phosphorylation of the chemotaxis protein CheY and its activity at the flagellar motor. Biochemistry 1992;31:1821–1826.
51. Appleby JL, Bourret RB. Proposed signal transduction role for conserved CheY residue Thr87, a member of the response regulator active-site quintet, J Bacteriol 1998;180:3563–3569.
52. Volz K, Matsumura P. Crystal structure of *Escherichia coli* CheY refined at 1.7 Å resolution, J Biol Chem 1991;266:15511–15519.
53. Roche P, Mouawad L, Perahia D, Samama J-P, Kahn D. Mo dynamics of the FixJ receiver domain: movement of the β4–α4 loop c with the in and out flip of Phe101. Protein Sci 2002;11:2622–2630.
54. Aqvist J, Medina C, Samuelsson JE. A new method for predicting affinity in computer-aided drug design. Protein Eng 1994;7:385–391.
55. Cui Q, Li G, Ma J, Karplus M. A normal mode analysis of structural plasticity in the biomolecular motor F1-ATPase. J Mol Biol 2004;340:345–372.
56. Li G, Cui Q. Analysis of functional motions in Brownian molecular machines with an efficient block normal mode approach: myosin-II and Ca^{2+}-ATPase. Biophys J 2004;86:743–763.
57. Ma J, Karplus M. The allosteric mechanism of the chaperonin groEL: a dynamic analysis. Proc Nat Acad Sci 1998;95:8502–8507.
58. Ma J, Karplus M. Ligand induced conformational changes in ras p21: a normal mode and energy minimization analysis. J Mol Biol 1997;274:114–131.
59. Johnson LN, Lewis RJ. Structural basis for control by phosphorylation. Chem Rev 2001;101:2209–2242.
60. Gsponer J, Haberthur U, Caflisch A. The role of sidechain interactions in the early steps of aggregation: molecular dynamics simulations of an amyloid-forming peptide from the yeast prion Sup35. Proc Natl Acad Sci USA 2003;100:5154–5159.
61. Masunov A, Lazaridis T. Potentials of mean force between ionizable amino acid sidechains in water. J Am Chem Soc 2003;125:1722–1730.
62. Yu ZY, Jacobson MP, Josovitz J, Rapp CS, Friesner RA. First-shell solvation of ion-pairs: correction of systematic errors in implicit solvent models. J Phys Chem B 2004;108:6643–6654.
63. Zhou R, Krilov G, Berne BJ. Comment on "Can a continuum solvent model reproduce the free energy landscape of a beta-hairpin folding in water?": the Poisson–Boltzmann equation. J Phys Chem B 2004;108:7528–7530.
64. Shukla D, Zhu XY, Matsumura P. Flagellar motor-switch binding face of CheY and the biochemical basis of suppression by CheY mutants that compensate for motor-switch defects in *Escherichia coli*. J Biol Chem 1998;273:23993–23999.
65. Zhu X, Volz K, Matsumura P. The CheZ-binding surface of chey overlaps the CheA- and FliM-binding surface, J Biol Chem 1997;272:23758–23764.
66. Schuster M, Abouhamad WN, Silversmith RE, Bourret RB. Chemotactic response regulator mutant CheY95IV exhibits enhanced binding to the flagellar switch and phosphorylation-dependent constitutive signalling. Mol Microbiol 1998;27:1065–1075.
67. Schuster M, Zhao R, Bourret RB, Collins EJ. Correlated switch binding and signaling in bacterial chemotaxis. J Biol Chem 2000;275:19752–19758.
68. Zhao R, Collins EJ, Bourret RB, Silversmith RE. Structure and catalytic mechanism of the *E. coli* chemotaxis phosphatase CheZ. Nat Struct Biol 2002;9:570–575.
69. Schuster M, Silversmith RE, Bourret RB. Conformational coupling in the chemotaxis response regulator CheY. Proc Natl Acad Sci USA 2001;98:6003–6008.
70. Lukat G, Lee B, Mottonen J, Stock A, Stock J. Roles of the highly conserved aspartate and lysine residues in the response regulator of bacterial chemotaxis. J Biol Chem 1991;266:8348–8354.
71. Welch M, Oosawa K, Aizawa S-I, Eisenbach M. Effects of phosphorylation, Mg^{2+} and conformation of the chemotaxis protein CheY on its binding to the flagellar switch protein FliM, Biochemistry 1994;33:10470–10476.
72. Knowles JR. Enzyme catalysis: not different, just better. Nature 1991;350:121–124.
73. Jardetzky O. Protein dynamics and conformational transitions in allosteric proteins. Prog Biophys Mol Biol 1996;65:171–219.
74. Benkovic SJ, Hammes-Schiffer S. A perspective on enzyme catalysis. Science 2003;301:1196–1202.
75. McElheny D, Schnell JR, Lansing JC, Dyson HJ, Wright PE. Defining the role of active-site loop fluctuations in dihydrofolate reductase catalysis. Proc Natl Acad Sci USA 2005;102:5032–5037.
76. Radkiewicz JL, Brooks CL. Protein dynamics in enzymatic catalysis: exploration of dihydrofolate reductase. J Am Chem Soc 2000;122:225–231.
77. Vale RD, Milligan RA. The way things move: looking under the hood of molecular motor proteins. Science 2000;288:88–95.
78. Houdusse A, Sweeney HL. Myosin motors: missing structures and hidden springs. Curr Opin Struct Biol 2001;11:182–194.
79. Rod TH, Radkiewicz JL, Brooks CL. Correlated motion and the effect of distal mutations in dihydrofolate reductase. Proc Natl Acad Sci USA 2003;100:6980–6985.
80. Mouawad L, Perahia D. Motions in hemoglobin studied by normal mode analysis and energy minimization: Evidence for the existence of tertiary t-like, quaternary r-like intermediate structures, J. Mol. Biol. 1996;258:393–410.
81. Xu CY, Tobi D, Bahar I. Allosteric changes in protein structure computed by a simple mechanical model: hemoglobin T → R2 transition. J Mol Biol 2003;333:153–168.
82. Vitkup D, Ringe D, Petsko GA, Karplus M. Solvent mobility and the protein "glass" transition. Nat Struct Biol 2000;7:34–38.
83. Fenimore PW, Franuenfelder H, McMahon BH, Parak FG. Slaving: solvent fluctuations dominate protein dynamics and functions. Proc Natl Acad Sci USA 2002;99:16047–16051.
84. Higo J, Sasai M, Shirai H, Nakamura H, Takaki K. Large vortex-like structure of dipole field in computer models of liquid water and dipole-bridge between biomolecules. Proc Natl Acad Sci USA 2001;98:5961–5964.
85. Royer WE, Pardanan A, Gibson QH, Peterson ES, Friedman JM. Ordered water molecules as key allosteric mediators in a cooperative dimeric hemoglobin. Proc Natl Acad Sci USA 1996;93: 14526–14531.
86. Zheng WJ, Brooks BR. Identification of dynamical correlations within the myosin motor domain by the normal mode analysis of an elastic network model. J Mol Biol 2005;346:745–759.
87. Fischer S, Windshugel B, Horak D, Holmes KC, Smith JC. Structural mechanism of the recovery stroke in the myosin molecular motor. Proc Natl Acad Sci USA 2005;102:6873–6878.
88. Ma J, Flynn TC, Cui Q, Leslie AGW, Walker JE, Karplus M. A dynamic analysis of the rotation mechanism for conformational change in fl-ATPase. Structure 2002;10:921–931.
89. Radhakrishnan R, Schlick T. Orchestration of cooperative events in DNA synthesis and repair mechanism unraveled by transition path sampling of DNA polymerase beta's closing. Proc Natl Acad Sci USA 2004;101:5970–5975.
90. Miyashita O, Onuchio JN, Wolynes PG. Nonlinear elasticity, proteinquakes, and the energy landscapes of functional transitions in proteins. Proc Natl Acad Sci USA 2003;100:12570–12575.
91. Ota N, Agard DA. Intramolecular signaling pathways revealed by modeling anisotropic thermal diffusion. J Mol Biol 2005;351: 345–354.
92. Im WP, Lee MS, Brooks CL. Generalized Born model with a simple smoothing function. J Comput Chem 2003;24:1691–1702.
93. Brooks BR, Bruccoleri RE, Olafson BD, States DJ, Swaminathan S, Karplus M. CHARMM: a program for macromolecular energy,

minimization and dynamics calculations. J Comput Chem 1983; 4:187–217.
94. MacKerell ADJ, Bashford D, Bellott M, Dunbrack RL Jr, Evenseck JD, Field MJ, Fischer S, Gao J, Guo H, Ha S, Joseph-McCarthy D, Kuchnin L, Kuczera K, Lau FTK, Mattos C, Michnick S, Ngo T, Nguyen DT, Prodhom B, Reiher WEI, Roux B, Schlenkrich M, Smith JC, Stote R, Straub J, Watanabe M, Wiórkiewicz-Kuczera J, Yin D, Karplus M. All-atom empirical potential for molecular modeling and dynamics studies of proteins. J Phys Chem B 1998;102:3586–3616.
95. Neria E, Fischen S, Karplus M. Simulation of activation free energies in molecular systems. J Chem Phys 1996;105:1902–1921.
96. Jorgensen WL, Chandrasekhar J, Madura JD, Impey RW, Klein ML. Comparison of simple potential functions for simulating liquid water. J Chem Phys 1983;79:926–935.
97. Almlof M, Brandsdal BO, Aqvist J. Binding affinity prediction with different force fields: examination of the linear interaction energy method. J Comput Chem 2004;25:1242–1254.
98. Lazaridis T, Karplus M. Effective energy function for proteins in solution. Proteins 1999;35:133–152.
99. Tama F, Sanejouand Y. Conformational change of proteins arising from normal mode calculations. Protein Eng 2001;14:1–6.
100. Hansson T, Marelius J, Åqvist J. Ligand binding affinity prediction by linear interaction energy methods. J Computer-Aided Mol Des 1998;12:27–35.